

NASA TECHNICAL MEMORANDUM



✓ NASA TM - 82494

OPTICAL STUDIES OF A MODEL BINARY MISCIBILITY GAP SYSTEM

✓ By L. L. Lacy, W. K. Witherow, B. R. Facemire,
and G. M. Nishioka
Space Science Laboratory

June 1982

NASA

*George C. Marshall Space Flight Center
Marshall Space Flight Center, Alabama*

(NASA-TM-82494) OPTICAL STUDIES OF MODEL
BINARY MISCIBILITY GAP SYSTEM (NASA) 54 p
HC 204/MF A01 CACL 14E

N82-33683

Unclas
G3/35 35105

1. REPORT NO. NASA TM-82494		2. GOVERNMENT ACCESSION NO.		3. RECIPIENT'S CATALOG NO.	
4. TITLE AND SUBTITLE Optical Studies of a Model Binary Miscibility Gap System				5. REPORT DATE June 1982	
				6. PERFORMING ORGANIZATION CODE	
7. AUTHOR(S) L. L. Lacy,* W. K. Witherow, B. R. Facemire, and G. M. Nishioka [†]				8. PERFORMING ORGANIZATION REPORT #	
9. PERFORMING ORGANIZATION NAME AND ADDRESS George C. Marshall Space Flight Center Marshall Space Flight Center, Alabama 35812				10. WORK UNIT NO. RTOP 179-80-60	
				11. CONTRACT OR GRANT NO.	
12. SPONSORING AGENCY NAME AND ADDRESS National Aeronautics and Space Administration Washington, D.C. 20546				13. TYPE OF REPORT & PERIOD COVERED Technical Memorandum	
				14. SPONSORING AGENCY CODE	
15. SUPPLEMENTARY NOTES Prepared by Space Science Laboratory, Science and Engineering Directorate *Exxon Prod. Research Co., Houston, TX 77001 [†] Owens Corning Fiberglas, Granville, OH 43023					
16. ABSTRACT In order to develop a better understanding of separation processes in binary miscibility gap metal alloys, model transparent fluid systems are being studied. The system selected was diethylene glycol-ethyl salicylate (DEG/ES) which has convenient working temperatures (288-350K), low toxicity, and is relatively easy to purify. The system is well characterized with respect to its phase diagram, density, surface and interfacial tensions, viscosity and other pertinent physical properties. Studies of migration of the dispersed phase in a thermal gradient were performed using conventional photo microscopy. Velocities of the droplets of the dispersed phase were measured and compared to calculated rates which included both Stokes and thermal components. A holographic microscopy system was used to study growth, coalescence, and particle motions. Sequential holograms allowed determination of particle size distribution changes with respect to time and temperature. Holographic microscopy is capable of recording particle densities up to 10^7 particles/cm ³ and is able to resolve particles of the order of 2 to 3 μ m in diameter throughout the entire volume of the test cell. Holography offers advantages over other optical techniques. The reconstructed hologram produces a wavefront that is identical to the original wavefront as it existed when the hologram was made. The reconstructed wavefront is analyzed using a variety of conventional optical methods.					
17. KEY WORDS Marangoni flow; droplet migration, holography, miscibility gap; phase separation			18. DISTRIBUTION STATEMENT Unclassified - Unlimited <i>Barbara R. Facemire</i>		
19. SECURITY CLASSIF. (of this report) Unclassified		20. SECURITY CLASSIF. (of this page) Unclassified		21. NO. OF PAGES 54	22. PRICE NTIS

TABLE OF CONTENTS

	Page
I. INTRODUCTION	1
II. PHYSICAL PROPERTY DATA FOR DIETHYLENE GLYCOL/ETHYL SILICYLATE	2
III. PARTICLE GROWTH/COALESCENCE STUDIES	3
A. Experimental Setup	3
B. Experimental Procedure	6
C. Results	7
IV. THERMAL MIGRATION STUDIES	8
A. Experimental Setup	8
B. Experimental Procedure	9
C. Results	9
V. CONCLUSIONS	11
REFERENCES	46

PRECEDING PAGE BLANK NOT FILMED

LIST OF ILLUSTRATIONS

Figure	Title	Page
1.	Refractive index, temperature-composition (ES-DEG)	12
2.	Refractive index, composition (ES-DEG)	13
3.	Ethyl salicylate-diethylene glycol phase diagram	14
4.	Density versus temperature for saturated phases, ES/DEG	15
5.	Surface tension (σ) versus temperature, various compositions of ethyl salicylate-diethylene glycol	16
6.	$\text{LN}\gamma_{\text{INT}}$ versus $\text{LN}(T_c - T)$ for ethyl salicylate-diethylene glycol	17
7.	Viscosity versus temperature for DEG and DEG-rich phase (saturated at 20°C)	18
8.	Viscosity versus temperature for ES and ES-rich phase (saturated at 20°C)	19
9.	Construction system	20
10.	Reconstruction system	21
11.	Bausch and Lomb automated feature-analysis Omnicon system	22
12.	Comparison of particle dispersions measured by the Omnicon system from normal microscopy techniques and holographic microscope techniques	23
13.	Different particle densities: 10^3 (top), 10^4 (center), and 10^5 (bottom) particles/cm ³	24
14.	Different particle densities in a 1-mm pathlength test cell	25
15.	Test cell	26
16.	10^7 particles/cm ³ in a 100- μm pathlength test cell	26
17.	Holographic isothermal test chamber	27
18.	Isothermal phase equilibration chamber	28
19.	Thermal history and holographic exposures for ES/DEG experiment ..	29
20a.	Particle size distribution; hologram No. 114	30
20b.	Particle size distribution; hologram No. 115	31
20c.	Particle size distribution; hologram No. 116	32

LIST OF ILLUSTRATIONS (Concluded)

Figure	Title	Page
20d.	Particle size distribution, hologram No. 117	33
20e.	Particle size distribution; hologram No. 118	34
21a.	Series of composite photographs taken from holograms at a magnification of 62X showing growth of the separating (ES rich) phase	35
21b.	Hologram No. 114, $t = 157.8$ sec, $\Delta T = 0.53$ K	36
21c.	Hologram No. 115, $t = 397.8$ sec, $\Delta T = 0.96$ K	37
21d.	Hologram No. 116, $t = 757.8$ sec, $\Delta T = 1.31$ K	38
21e.	Hologram No. 117, $t = 1297.8$ sec, $\Delta T = 1.49$ K	39
21f.	Hologram No. 118, $t = 2017.8$ sec, $\Delta T = 1.57$ K	40
22.	Measured particle motion in various parts of the test cell	41
23.	Schematic of immiscible fluid thermal migration apparatus	42
24.	Relative effects of thermal and concentration gradients on interfacial tension driven droplet motion	43

LIST OF TABLES

Table	Title	Page
1.	Densities of Ethyl Salicylate-Diethylene Glycol Solutions	44
2.	Comparison of Measured and Calculated Velocities for Selected Drops	45
3.	Values of V_c/V_m Obtained with Maximum Measurement Errors of Velocity and Radius	45

TECHNICAL MEMORANDUM

OPTICAL STUDIES OF A MODEL BINARY MISCIBILITY GAP SYSTEM

I. INTRODUCTION

Immiscible materials are liquids that have limited mutual solubility. Immiscible liquid systems, commonly called emulsions, occur in a wide variety of chemical processes and products. Such processes as latex formation, waste water treatment, enhanced oil recovery, and the manufacture of products such as paints and photographic films involve emulsions. Emulsions also play an important role in certain biological systems. Thus, an increased understanding of immiscible liquid systems would be useful to a wide variety of industries.

Within NASA, two-component metallic systems with a liquid phase miscibility gap are currently of interest because of recent space processing experiments [1,2]. Occasionally new materials composed of homogeneous combinations of solid dispersed materials are found to exhibit new characteristics. For example, bulk properties such as superconductivity and semiconductor-like behavior were found to depend on the fineness of the dispersed phase in the immiscible alloy [3,4].

The formation of immiscible alloys involves a complex series of events. On cooling an initially homogeneous metallic melt through its miscibility gap, the processes of nucleation, growth, coalescence, and solidification successively affect the ultimate structure of the alloy. Each of these processes is, in turn, affected by factors such as cooling rate, surface energies, convection, and sedimentation. The ultimate structure of an alloy is path dependent, so a complete understanding of solidification requires knowledge of structure throughout the cooling process. Because of the opaqueness of metals, investigations of metallic monotectic alloys are handicapped since they can only analyze the final alloy structure. A way around this problem is to design a model immiscible composed of transparent materials (e.g., organics, H_2O , etc.) [5,6]. This type of system can then be observed using optical techniques. Advantages of studying model materials include convenient experimental conditions which are relatively easy to control, and their transparency allows continuous observation of the entire cooling process. Thus, nucleation, growth, coalescence, bulk phase separation, fluid transport, and solidification effects can each be studied separately and their influence on ultimate structure deduced.

There are two basic methods of two phase formation from the homogeneous phase, nucleation and spinodal decomposition [7,8]. Nucleation is said to occur when the dispersed phase forms spherical shapes, which it does by overcoming an energy barrier and forming around a nucleus. Spinodal decomposition occurs when a solution is cooled into the spinodal region of the phase diagram and nucleation has not taken place. The dispersed phase in this case forms as thin alternating regions within the congruent phase. As the two phases separate, the denser fluid will begin to sink to the bottom of the test cell due to gravity. On Earth, in systems with relatively large density differences between the two phases, buoyant forces are a major cause of phase separation.

The phase that has formed spherical shapes, or particles, will continue to increase in size by certain growth processes. Methods of growth include diffusional growth, coalescence, and Ostwald ripening. Diffusional growth occurs when the previously nucleated particles continue to absorb the solute material out of the matrix phase. Coalescence is an important factor in that two particles that collide will combine to form a larger particle. Finally, Ostwald ripening, a process that was discovered by W. Ostwald around 1900 [9], is a process in which small particles tend to diffuse back into the matrix phase; the larger particles tend to preferentially grow by diffusion. The larger particles thus absorb the solute material out of the host phase. In other words, small particles become smaller and large particles become larger.

By reducing gravity to 10^{-4} g as in an orbiting spacecraft, buoyancy driven separation is virtually eliminated. However, in the reduced gravity environment, separation processes which were of less significance on Earth become the dominating effects. Several solidification experiments were performed in low gravity in which separation was much greater than would be expected based solely on buoyant forces [10,11]. In a demonstration of emulsion stability in low-g on Skylab, Krytox oil ($\rho = 1.86 \text{ g/cm}^3$) and water showed no tendency to separate [12]. No thermal, solutal, or solidification effects were operative in this demonstration. Thus, it is postulated that these effects caused the unwanted separations obtained in the solidification flight experiments.

In order to better understand these separation processes, the model system, Ethyl Salicylate-Diethylene Glycol (ES/DEG), is being used to study phenomena occurring inside the miscibility gap. This report covers the results of two types of optical studies designed to investigate separation phenomena:

- 1) A holographic system was used to study growth, coalescence, and particle motions. Sequential holograms were taken as the sample was cooled below the coexistence curve. From these holograms particle size distributions with respect to time and temperature were determined. Resolution of particles from 2 to 3 μm is possible from the hologram.
- 2) Conventional photomicroscopy was used to study thermal migration of the dispersed phase. Upward velocities of the more dense phase (induced by variations of the interfacial tension with temperature) were measured and compared with theory.

II. PHYSICAL PROPERTY DATA FOR DIETHYLENE GLYCOL/ETHYL SALICYLATE

Diethylene glycol and ethyl salicylate are relatively safe to handle, non volatile, easy to purify, and the system has a convenient working temperature range ($< 345 \text{ K}$). The low working temperatures allow the use of water baths for temperature control.

Commercial reagent grade materials purchased from Fisher were purified by vacuum distillation. Each material was distilled through a packed column three times and the middle fraction was collected. The final fractions were collected at 7 torr at $370.3 \pm 0.2 \text{ K}$ (ethyl salicylate) and $395.3 \pm 0.2 \text{ K}$ (diethylene glycol).

The phase boundary for this system was determined by refractive index measurements and by clear point observations near the critical solution temperature. A calibration curve of refractive index versus composition and temperature was prepared in order to measure the phase diagram. Figures 1 and 2 show these refractive index curves. The phase diagram determined by this technique is shown in Figure 3. Reference 13 gives further details of this work.

A Westphal balance was used to determine densities of various solutions of DEG/ES from 0 to 100 mole % ES versus temperature. A jacketed cell through which water was circulated to control temperatures contained the sample. The cell was placed in a chamber purged with filtered dry nitrogen. Tables I(a) and (b) give the results of these measurements. Figure 4 shows graphically the density differences for the saturated phases versus temperature.

A sample cell and dry nitrogen chamber similar to that used in the density measurement work was utilized in obtaining surface tensions of the DEG/ES system. Immediately prior to measurement, the surface of the fluid was skimmed off using a pipette connected to a vacuum pump through a cold trap to prevent back diffusion of oil. This removed any surface contaminants. A DuNouy ring suspended from a Cahn electrobalance was used to measure the surface tensions. Figure 5 shows surface tension with respect to temperature for various compositions of DEG/ES.

The same apparatus was used to measure interfacial tensions. The two phases were allowed to equilibrate in the thermostated sample container. The DuNouy ring was passed through the interface to make a measurement. Figure 6 presents the results of these measurements. The interfacial tension was found to be

$$\gamma_{\text{int}} = 9.15 \times 10^{-3} (T_c - T)^{1.36} ,$$

so that

$$d\gamma/dT = -1.2444 \times 10^{-2} (T_c - T)^{0.36} .$$

A Wells-Brookfield microviscometer was used to measure viscosity. The sample cup of this viscometer is jacketed so that viscosity versus temperature can easily be measured. This instrument gives accuracies of ± 1 percent of the range used. The spindle and rotation speed used in a measurement determine the range. Viscosity versus temperature of four compositions were measured: pure DEG, pure ES, and the two equilibrium phases at 20°C. The latter two were the compositions used in the thermal migration studies described in Section IV of this report. Figures 7 and 8 show the results of these measurements.

III. PARTICLE GROWTH/COALESCENCE STUDIES

A. Experimental Set up

1. Holographic Techniques. Holography is unique in that it records both amplitude and phase information from the test cell [14]. In doing this, the wavefront that was coming from the test cell at the time the hologram was made is stored in a photographic material permanently. When the hologram is reconstructed, the identical wavefront is reproduced; in other words, an exact three-dimensional image of the object is obtained. This reconstructed image can then be investigated by several optical techniques. For example, microscopy can be used except that now the entire test cell can be investigated for each moment of time that a hologram was taken. Thus, by investigating the image of the test cell from a hologram, the limitations of normal microscopy (i.e., small field of view and narrow depth of focus) are eliminated.

Holography has long been used to measure small particles [15-19]. Holograms are usually made from the interference between two beams of laser light, an object beam, and a reference beam. The object beam is made incident on the object where the laser light is randomly phase-shifted. The reference beam is unchanged so that when the two beams coincide on the film, they interfere with one another and create a hologram. Then, when the developed film is re-illuminated with the reference beam, a three-dimensional image of the object is obtained.

The following in-line holographic system was used to investigate the dynamics of immiscible fluids [20] (Fig. 9). The laser used in the construction system was a Coherent Radiation argon ion laser. The wavelength used was $0.5145 \mu\text{m}$ at a power of 1 W. The output was in the TEM_{00} mode and the coherence length of the laser was approximately 1 m. The laser beam passes through a spatial filter which produces a uniformly intense expanding beam of light. A collimating lens (focal length 100 mm, diameter 42 mm) is used to collect the expanding beam and collimate it. The collimating lens has a properly matched focal length and diameter so that almost 100 percent of the expanding beam from the spatial filter is converted to the collimated beam. Using such a lens aids in keeping the light intensity reaching the film as high as possible so that exposure times can be kept short. The collimated light then passes through a focusing lens (focal length 50 mm, diameter 63 mm) where the beam is focused. The test volume lies between the focal point of the focusing lens and the film plane. The focusing lens and the spatial filter each produce divergent beams of light. However, the angle of divergence is greater from the focusing lens than it is from the spatial filter. It was determined experimentally that it is the greater angle of divergence that improves the resolution of this system over conventional in-line holographic microscopy systems.

While this apparatus has a resolution of $2 \mu\text{m}$, there are two disadvantages (1) the cone of light from the focusing lens limits the maximum test volume size and (2) optical aberrations are created. Coma aberration is caused by the large degree of curvature of the focusing lens. The farther off the optical axis that the particles lie, the more severe the aberration becomes. However, the aberration can be corrected during the reconstruction of the hologram.

The holographic reconstruction system that was used to reconstruct and magnify the holograms taken in the construction system is diagrammed in Figure 10. The laser used in the reconstruction system is another argon ion laser with the same characteristics as the one used in the construction system. The laser beam passes through a spatial filter to produce a uniform-intensity, expanding beam that is incident upon the vidicon tube of a television camera. The hologram to be reconstructed is positioned near the spatial filter. In this manner a real image of the test cell is produced from the hologram and is projected onto the television camera. The depth of focus of this system was determined empirically to be on the order of $100 \mu\text{m}$. Since the test cells used for these tests have a path length of $100 \mu\text{m}$, the entire depth of the cell can be examined without moving the hologram along the optical axis of the reconstruction system. By moving the hologram in the x-y directions of the plane of focus, the entire volume of the test cell can be investigated.

Note that there are no lens between the test cell and film in the construction system or between the film and the television camera in the reconstruction system. The hologram itself can be considered to act as a lens that contributes the reconstruction magnification of the system with the television camera contributing electronic magnification. The remaining portion of the overall magnification comes from the divergent beam used in the construction system. Since the hologram acts as a lens, different magnifications result when moving the hologram along the optical axis to

view the different portions of the test cell. This variation of magnification can be accounted for and is described in detail in a previous paper [21]. The reconstruction system has a range of magnification ranging from 1X to about 1200X even though no magnification lens are used.

As was mentioned earlier, aberrations are introduced into the hologram from the focusing lens that is used. These aberrations can be minimized through proper reconstruction techniques [22]. The construction system causes positive coma in the particles that are not on the optical axis. By reconstructing the test cell image through the same lens, negative coma of the proper magnitude can be introduced. The positive coma and negative coma cancel each other, thus correcting this type of aberration.

The equipment used to measure the size distribution of the particles is built by Bausch and Lomb and is known as the Omnicon Automated Feature Analysis System (Fig. 11). It is composed of a computer processor, the sizing electronics, television camera and monitor, gray level threshold box, CRT-keyboard, and a line printer. The image incident on the vidicon tube produces corresponding voltages in the tube which are sent to the sizing electronics. When the voltage of a camera scan line exceeds a particular threshold voltage set by the gray level threshold box, that part of the image is identified as a feature to be measured. This system is capable of measuring different types of parameters, such as area (including or excluding holes), longest dimension, projected length, and Feret's diameter.

The optics system was tested to determine its ability to record and measure a particle distribution. A comparison test between normal microscopy and holographic microscopy was devised. The Omnicon system has an automated microscope with which samples can be measured automatically. The microscopy stage has motorized x-y axes translators which are controlled by the computer. Samples of glass spheres of unknown size were placed on a microscope slide and measured with the Omnicon system. About 90,000 particles were counted to obtain a good statistical distribution. Next a quantity of the same spheres was suspended in silicone oil in a test cell and a hologram was taken. After the reconstruction system had been calibrated, the hologram containing the glass spheres was measured by the Omnicon system. The distributions measured by normal microscopy and holographic microscopy are seen to be in good agreement (Fig. 12).

Another important test was to determine the highest particle density that could be recorded. Holograms were made of the following particle densities, 10 , 10^2 , 10^3 , 10^4 , and 10^5 particles/cm³. The particles were contained in a test cell that was 1 cm in depth along the optical axis. The holograms were examined in the reconstruction system for the quality of the image (Fig. 13). It is seen that the best holograms were produced at particle densities less than or equal to 10^3 particles/cm³, fair holograms at 10^4 particles/cm³, and poor holograms at 10^5 particles/cm³.

Higher particle densities should be possible if the path length is reduced. To test this, a 1-mm path length test cell was obtained and the following particle densities used, 10^3 , 10^4 , 10^5 , and 10^6 particles/cm³. By decreasing the volume by one order of magnitude, the highest particle density that could be recorded increased by one order of magnitude (Fig. 14).

2. Test Apparatus. DEG has a density of 1.12 gm/cm^3 and an index of refraction of 1.447, while ES has a density of 1.13 gm/cm^3 and an index of refraction of 1.523 [23]. The only requirement of the indices of refraction of the two liquids is that they differ at least on the order of 0.01. If the indices of refraction were identical, the laser light would not be diffracted by the separating phase and thus would not be observed.

Calculations indicated that particle densities of 10^5 to 10^7 particles/ cm^3 could be expected. Since by decreasing the path length of the test cell, higher particle densities could be holographed, a test cell of 100- μm thickness along the optical axis was selected (Fig. 15). The reconstructed holograms show particle densities that are calculated to be of the order of 10^7 particles/ cm^3 (Fig. 16). Thus, by using thin test cells, extremely high particle densities can be used. It is recognized that, with such thin cells, wall effects may become significant. However, the majority of the particles do not nucleate on the walls and are small enough ($< 20 \mu\text{m}$) that wall effects are not felt to be a severe problem in this study.

Temperature control of this experiment is very important. A temperature gradient across the test cell may cause particle motion by convection which could interfere with the mechanisms of separation and growth. To produce an isothermal environment, the test cell was placed in a temperature bath (Fig. 17). The temperature bath is a plexiglass box encased in insulating material with two optical windows. A stirrer is placed in the temperature bath so that the water is well stirred. A circulating water bath is used to control temperature. The thermometer used to measure the temperature in the bath is a Hewlett-Packard quartz thermometer that has an accuracy of 0.1 mK.

The temperature control system that was used to regulate the temperature of the water bath was an RTE-8 refrigerated circulating bath that is built by the Neslab Corporation. The water is continuously filtered through a 0.2 micron filtering system. The filtering system is a passive filter and is available from the Millipore Corporation. With this system, the temperature bath is stabilized to $\pm 0.5 \text{ K}$.

B. Experimental Procedure

To obtain a sample for the experiment, approximately equal amounts of purified DEG and ES were added in an isothermal separating chamber (Fig. 18). The isothermal separating chamber has a thermal jacket controlled by a temperature bath. The temperature of the bath was set above the consolute temperature so that the two fluids would mix completely. The temperature was then lowered to a point on the DEG-ES phase diagram that was to be investigated. After a day, the fluid in the separating tube would be separated into two layers. The top layer would be DEG rich and the bottom layer would be ES rich. For example, if the temperature of the bath had been set at 298 K, the top layer would be 19 mole % ES, while the bottom layer would be 92 mole % ES. The top layer is then drawn off and loaded into a test cell. The cloud point temperature of this example would be 298 K (Fig. 3).

The temperature in the water bath in the optics system is kept above the temperature at which the test sample fluid was drawn out of the separating tube. After a few hours at this elevated temperature, the temperature of the bath and test cell have stabilized. The temperature is then quenched to just below the cloud point temperature. It is at this point that the nucleation, separation, and growth will occur.

A reference hologram is made of the test cell after the fluids have stabilized at the temperature above the cloud point temperature. As the temperature is decreased, a few holograms are taken to ensure nothing occurs above the cloud point temperature. When the temperature below the cloud point temperature is reached, a hologram is taken about every minute (Fig. 19). The actual exposure time of each hologram is 3 to 5 msec. The film that is used is Agfa-Gaevert 10E-56 high-resolution holographic film. The development process of this film is a standard black and white film development procedure; details of this process are found in Reference 20.

C. Results

The developed holograms were placed in the reconstruction system and analyzed with the Omnicon system. One particular sequence of holograms demonstrates nucleation, diffusional growth, and coalescence (Fig. 20 a through e). [Each figure corresponds to holograms 114 through 118 shown in the thermal history curve (Fig. 19). As can be seen, at no time during this series was the cell in thermodynamic equilibrium, since the temperature drops throughout the entire series.] In this particular example, Figure 20a shows nucleation and the early growth of the separating phase. Figures 20b, 20c, and 20d demonstrate growth by diffusional processes; that is, the separated phase grows by absorbing more solute out of the matrix phase. Figures 20b and 20c also indicate the nucleation of new particles. Notice that Figure 20d contains a higher number of particles at its peak than Figure 20c does. However, the overall width of Figure 20c is wider than Figure 20d. What has probably occurred is that the particles in the 12- to 14- μm diameter region grew at a faster rate than the particles in the 14- to 18- μm diameter region of Figure 20c. That is, the smaller particles grew faster than the larger particles, thus creating the larger, narrower peak of Figure 20d. This is the opposite observation which one would expect with Ostwald Ripening; however, this system was being cooled and was not in thermal equilibrium. Finally, Figure 20e demonstrates coalescence. Instead of one fairly sharp peak as in Figure 20d there are now three distinct peaks; this is caused by the coalescence of particles. That is, the sharp single peak in Figure 20d has been depleted by some of the particles in that peak combining with other particles to form two peaks that are apparent in Figure 20e.

Growth rates can be calculated from the graphs obtained. For example, Figure 20d peaks at 10 μm , while Figure 20c peaks at 14 μm ; the separation of time between the two holograms that the curves were taken from is 6 min. Thus, the growth rate is found to be 11 nm/sec. The nucleation and growth of the separating phase can be observed directly from photographs taken from the series of holograms 113 through 118 (Figs. 21a through f). These photographs are composites of pictures that cover approximately 0.07 cm^2 of a 1.58 cm^2 test cell. Figure 21a shows the test cell at a time the temperature was above the cloud point temperature when the two fluids were mixed in a homogeneous solution. Figure 21d shows particle growth again, and one can begin to detect some particle motion. Figure 21e again depicts particle growth, but now particle motion is readily detected. Finally, Figure 21f shows more particle growth and motion and coalescence of particles.

Particle motion can also be demonstrated from holograms 114 to 118. Series of photographs were taken from different locations of the test cell. By placing plastic overlays over the photographs and charting the subsequent positions of the particles, particle motion is shown (Fig. 22). Particle velocities can be calculated using the time separation between the holograms.

IV. THERMAL MIGRATION STUDIES

Several factors influence the separation of a two-phase partially miscible liquid system cooled below its coexistence curve. As drops of the dispersed phase form during cooling their density becomes different from the matrix phase since these two phases now have different chemical compositions. In a gravity environment this density difference is generally a major cause of separation as the lighter material rises and the heavier one sinks. In the absence of a gravity field, or in a very weak one, such buoyancy effects become negligible and other factors predominate.

One of the effects which becomes a strong consideration in low-g is motion of the drops due to variations in interfacial tension from one side of the drop to the other. This motion can lead to separation of the two phases as does settling of the heavier phase in one-g. Two phenomena leading to an interfacial tension gradient are the existence of thermal gradients in the system and the presence of concentration gradients. Partially miscible systems subjected to a thermal gradient experience both of these phenomena since concentration is temperature dependent.

The experiments and analysis reported here consider only thermal interfacial tension gradient effects, although it is agreed that concentration effects also influence the motion of the drops. A more thorough analysis of concentration effects is planned in future studies. The present work shows that interfacial tension gradients are a significant mechanism of separation in a two liquid phase system and that the existing theory of thermal migration at least qualitatively predicts the magnitude of the effect.

The DEG/ES system is an excellent one for ground-based studies of thermal migration. The density differences of the two phases are small enough so that the Stokes velocity of small drops of the heavier ES-rich phase is rather slow allowing the observation of other effects. Interfacial tension gradients as a function of temperature are sufficient to give thermal migration velocities an order of magnitude greater than the calculated Stokes velocity.

A. Experimental Setup

The samples were prepared by mixing purified DEG and ES at near the critical composition in the jacketed separatory funnel described in a previous section of this paper. Circulating hot water from a water bath around the funnel heated the mixture into the homogeneous region. The bath temperature was then lowered to 293 K and the phases allowed to settle and equilibrate for at least 24 hr. All runs reported in this section used the top phase (DEG-rich) at 293 K. By using this composition, heavier ES-rich drops will form when the solution is cooled below 293 K. Under isothermal conditions, these drops settle slowly. In a temperature gradient any upward motion not accompanied by a prevailing convective pattern is attributed to interfacial tension gradient effects.

Figure 23 shows the apparatus used for these experiments. A standard 1 × 1 cm spectrophotometer cell contained the sample. The base for the cell was a thermoelectric device, providing a controllable cold plate. A water cooled heat sink removed waste heat from the thermoelectric device. A specially designed stainless steel plug, threaded at the top, fit into the cell and served as the hot plate. A standard soldering iron and rheostat controlled the hot plate temperature. The plug passed through a teflon fitting to minimize heating of the glass walls of the cell. A copper/constantan thermocouple inside the hot plate and one adjacent to the bottom

of the cell monitored temperatures. Heating from the top and cooling from the bottom stabilized the system against buoyancy-driven convection.

A Carl Zeiss stereo microscope was the imaging system for a 16-mm Bolex camera which operated at 12 frames per second to record the motion of ES-rich drops in the DEG-rich matrix fluid. A field of view of approximately 2×3 mm was obtained. A wire of known diameter was photographed inside the fluid after the tests to obtain exact magnification factors.

B. Experimental Procedure

A typical experiment consists of filling the cell with homogeneous DEG/ES solution and positioning the cell on the cold plate. Careful insertion of the hot plate eliminates trapped air bubbles which would interfere with the heat transfer from the hot plate. The temperature gradient is established and allowed to equilibrate. Almost immediately after imposing the gradient, a cloud of ES-rich particles forms in the lower part of the cell. This cloud is initially so densely populated by small particles that, with the optics used, they can not be individually observed. However, as the particles grow and the gradient becomes established, the particles begin to move upward against gravity into a thinly populated area where their motions are filmed. The temperatures are recorded periodically until steady state is reached. After focusing on drops in the field of view, photography begins. Knowing the frame rate and the magnification factor, drop sizes and velocities are determined from the film.

C. Results

If the direction of the gravity vector is taken as positive, then the velocity of a droplet in a thermal gradient is given by the expression [24,25],

$$V = \frac{2}{3\mu(3\mu' + 2\mu)} \left[\left(-\frac{d\gamma}{dT} \right) RT_c \mu + (\rho' - \rho) gR^2(\mu + \mu') \right]$$

where

$$T_c = \frac{3 dT/dx}{2 + h/h'}$$

μ and μ' = the viscosities of the matrix and dispersed phases respectively,

ρ and ρ' = their densities,

h and h' = thermal conductivities,

R = radius of a drop,

$d\gamma/dT$ = interfacial tension gradient with respect to temperature

dT/dx = thermal gradient and

g = the acceleration due to gravity .

The R term reflects thermal velocity and the R^2 term the Stokes contribution. The small drops in these experiments and the small density differences involved ($\Delta \rho \sim 0.005 \text{ gm/cm}^3$) result in the Stokes term being at least an order of magnitude smaller than the thermal term. Assuming equal thermal conductivities of the two phases ($h = h'$) then $T_c = dT/dx$.

A linear temperature profile was assumed in calculating fluid properties and expected velocities. Actual velocities are generally less than calculated values. In other words, the drops move more slowly in the upward direction (toward the hot plate) than they should according to the theory used. Table 2 shows the calculated and actual velocities for several drops. The ratio, $V_{\text{calculated}}/V_{\text{measured}}$ (V_c/V_m) is also given and is used as an index of agreement between theory and experimental results. Measured velocities are in good qualitative agreement with the theory. Discrepancies between V_c and V_m can be explained by several factors and further experiments are planned to account for these. A brief discussion of the influencing parameters and their effect on the experimental results follows.

Experimental measurements which are potential sources of error are (1) temperatures of the hot and cold plates, (2) drop radius, and (3) drop velocity. Inaccuracies in temperature measurements will lead to an error in the dT/dx used; the implications of this are the same as those of assuming a linear profile. The drop radius measurement is accurate to $\pm 1.8 \mu\text{m}$ and the velocity to $\pm 1.42 \times 10^{-4} \text{ cm/sec}$. Magnification differences caused by viewing through different depths of fluid were minimized by measuring the velocities of drops in approximately the same focal plane. Table 3 indicates the effect of measurement error on V_c/V_m for a given drop, nominal $R = 20.9 \mu\text{m}$ and nominal measured velocity = $1.43 \times 10^{-3} \text{ cm/sec}$. Maximum error caused by experimental error in velocity and radius measurement is ± 20 percent.

The present apparatus does not allow for a direct check of the temperatures inside the fluids; so a linear thermal profile was assumed between the hot and cold plates. Since the hot and cold plate temperatures bracketed the ambient temperature, heat losses which would lead to a nonlinear profile were minimized. A nonlinear profile near the hot plate would affect the velocities observed, because all the drops were within 1 to 2 mm of this plate. Since the Stokes component is independent of dT/dx (except for variations of $\Delta \rho$), the effect is limited to the thermal velocity which is an order of magnitude greater than the Stokes contribution. Referring to the velocity equation, it can be seen that the velocity is proportional to any variance in dT/dx . The gradient was measured on the outside of the cell between the cell wall and the insulation to arrive at an estimate of the nonlinearity existing in the fluid. An error of approximately ± 10 percent is possible from the assumption of a constant gradient.

The mismatch between the thermal conductivities of the glass cell walls and the DEG/ES and the fact that two walls are not insulated lead to nonlinear isotherms within the test volume. This is evidenced by a bowed cloud front during the experiment. A residual convective flow caused by this condition would affect velocities. If such flow is present, its magnitude is significantly less than the thermally induced drop motion since in no area of the cell were drops seen with a downward velocity. Experiments using neutrally buoyant tracer particles should clarify the existence of any slow convective pattern caused by nonlinear isotherms. Improvements in cell design may reduce this problem. A KC-135 flight experiment is also planned which will eliminate convective effects. Equilibrium values of property data were used for

the calculations. Future work is planned to determine the effects of nonequilibrium conditions on the properties used (ρ , μ , h , and γ).

As drops of ES-rich phase move toward the hot plate in the thermal gradient, they are at temperatures above the coexistence curve and are, therefore, slowly dissolving in the DEG-rich matrix fluid as they rise. Refractive index changes caused by concentration differences resulting from this dissolution appear as faint plumes behind the drops. An area of higher ES concentration on the cold side of the drop would decrease the interfacial tension on that side retarding the upward velocity as indicated in Figure 24. Actual drop velocities, being slower than the calculated values, are consistent with this possibility. Therefore, this is considered an important factor in these experiments, since the velocity is proportional to interfacial tension gradients. Further studies are planned to clarify the magnitude of such solutal effects.

V. CONCLUSIONS

The use of model transparent fluid systems allows the study of phase separation processes by optical techniques not applicable to opaque systems. Holographic microscopy is a useful method of studying a variety of growth mechanisms of the dispersed phase including coalescence and diffusional growth. Particle motions can also be observed. Holography offers the advantage over other methods of being able to observe individual droplets over the entire test volume at any given moment during an experiment. A disadvantage of the method, as applied to two phase systems, is the limitation of the light path to about 100 μm which increases the possibility of wall effects.

Thermal migration velocities of droplets of the dispersed phase have been shown to agree qualitatively with the theory of Young, et al. Drops of the more dense ES-rich phase migrated upward against gravity in an imposed thermal gradient effectively demonstrating that Marangoni forces can be a substantial influence in phase separation processes. Although the drops move more slowly than predicted, these discrepancies between experiment and theory are explainable in terms of the following:

- 1) Uncertainties introduced by using property data, measured with equilibrium phases, under non-equilibrium conditions
- 2) The validity of assuming a linear thermal profile within the cell
- 3) Residual Rayleigh-type convection
- 4) Concentration gradients caused by solutal effects.

Experiments with more rigid control are needed to elucidate the influence of these factors.

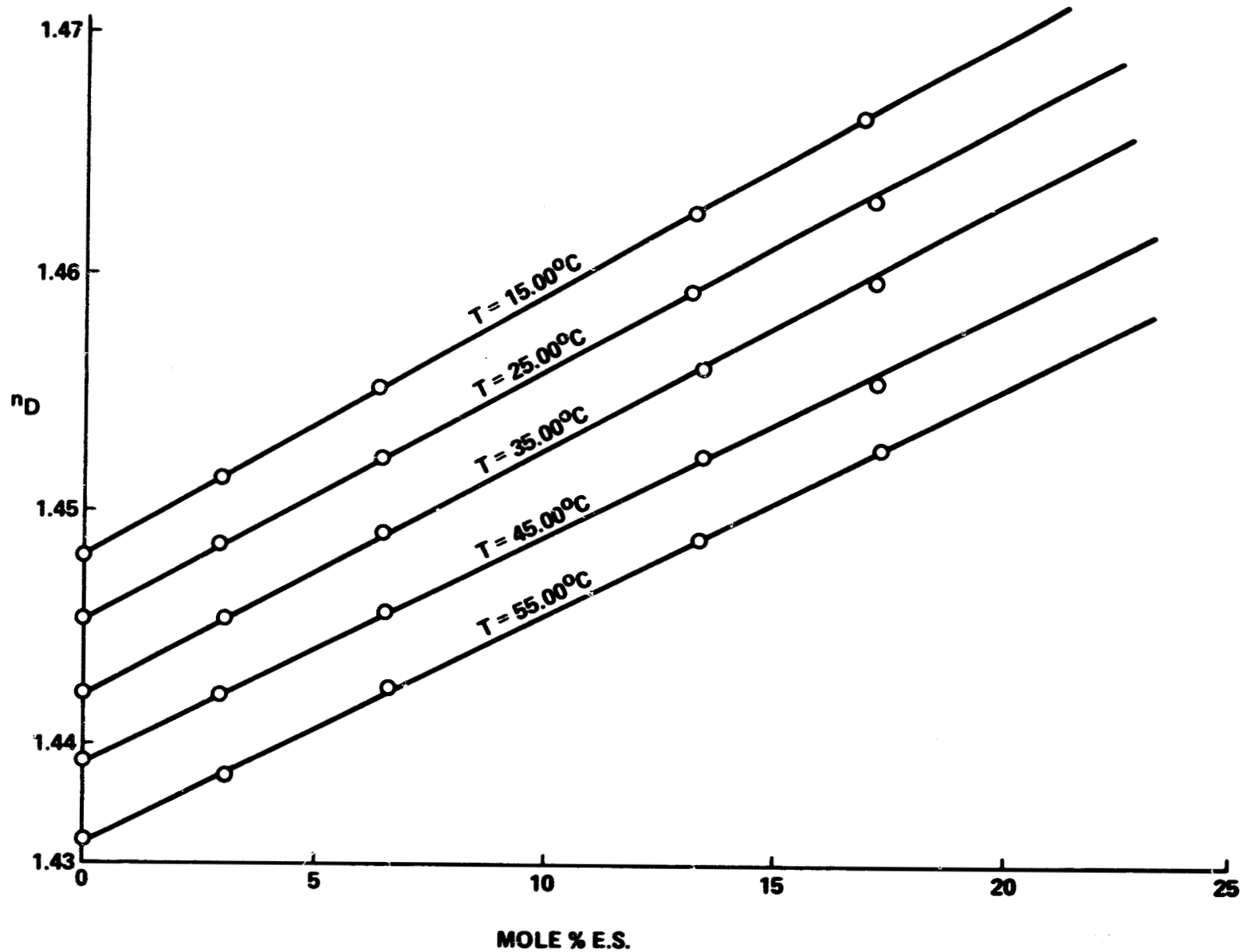
ORIGINAL PAGE IS
OF POOR QUALITY

Figure 1. Refractive index, temperature-composition (ES-DEG).

ORIGINAL PAGE IS
OF POOR QUALITY

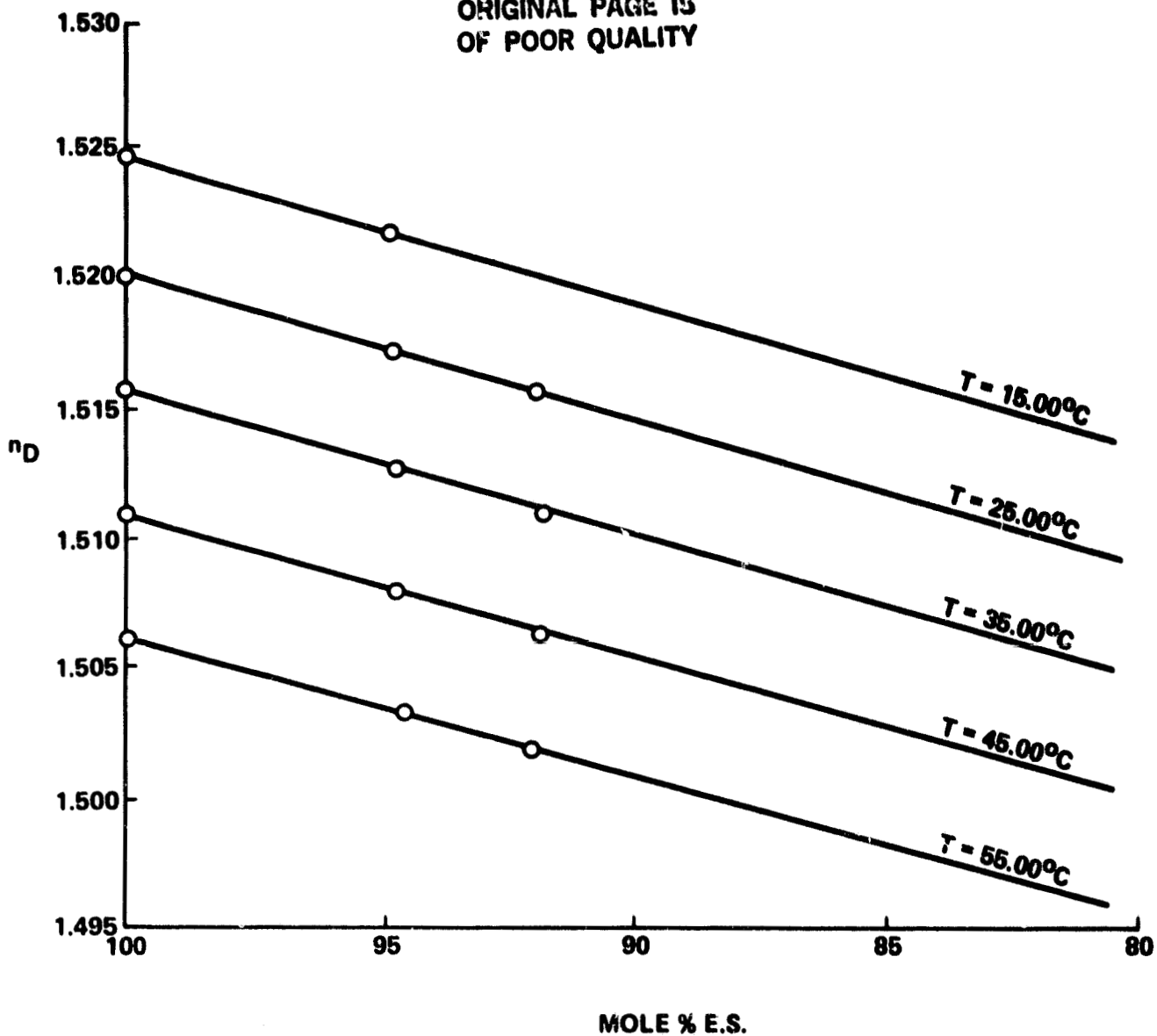


Figure 2. Refractive index, composition (ES-DEG).

ORIGINAL PAGE IS
OF POOR QUALITY

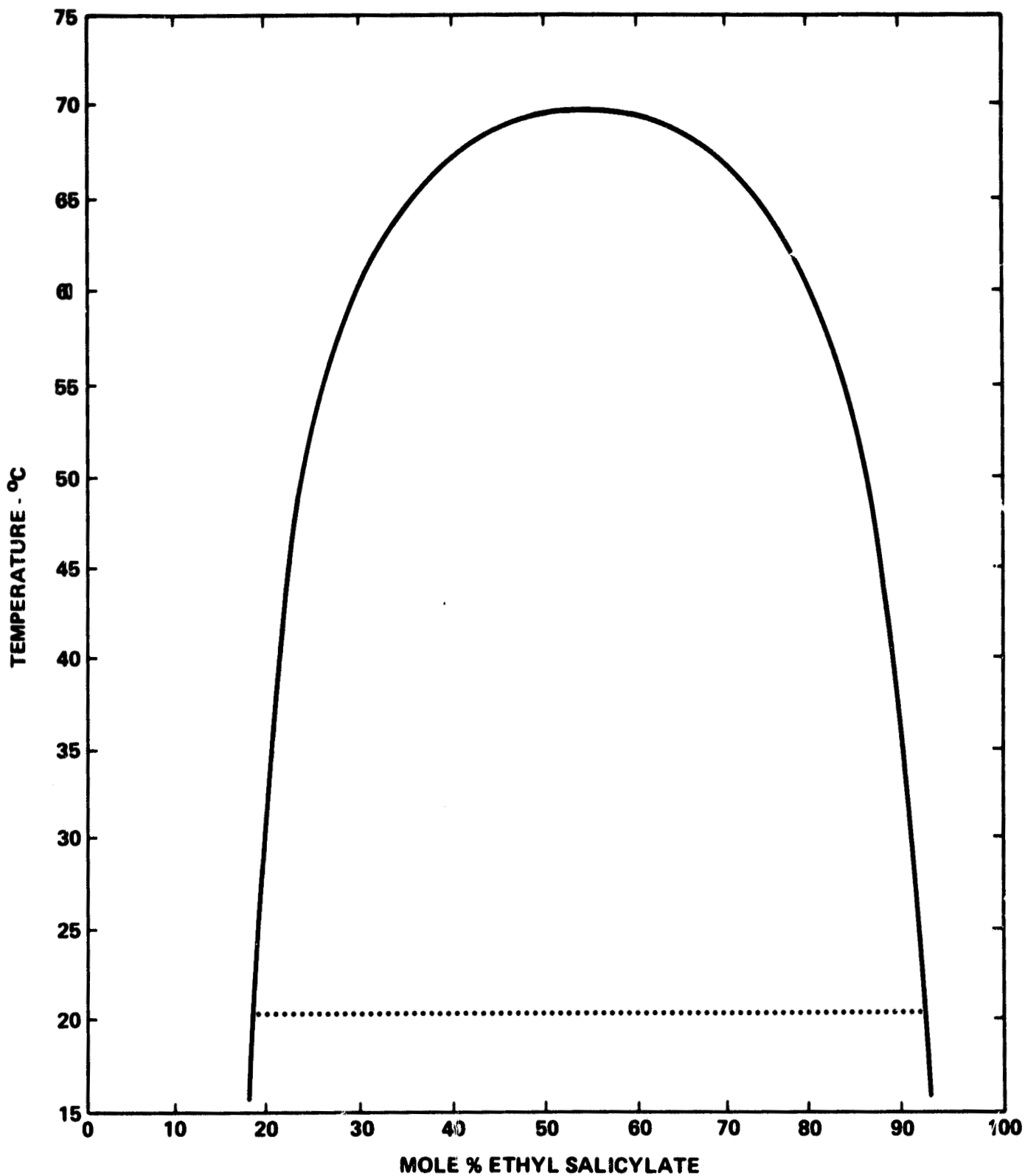


Figure 3. Ethyl salicylate-diethylene glycol phase diagram.

ORIGINAL PAGE IS
OF POOR QUALITY

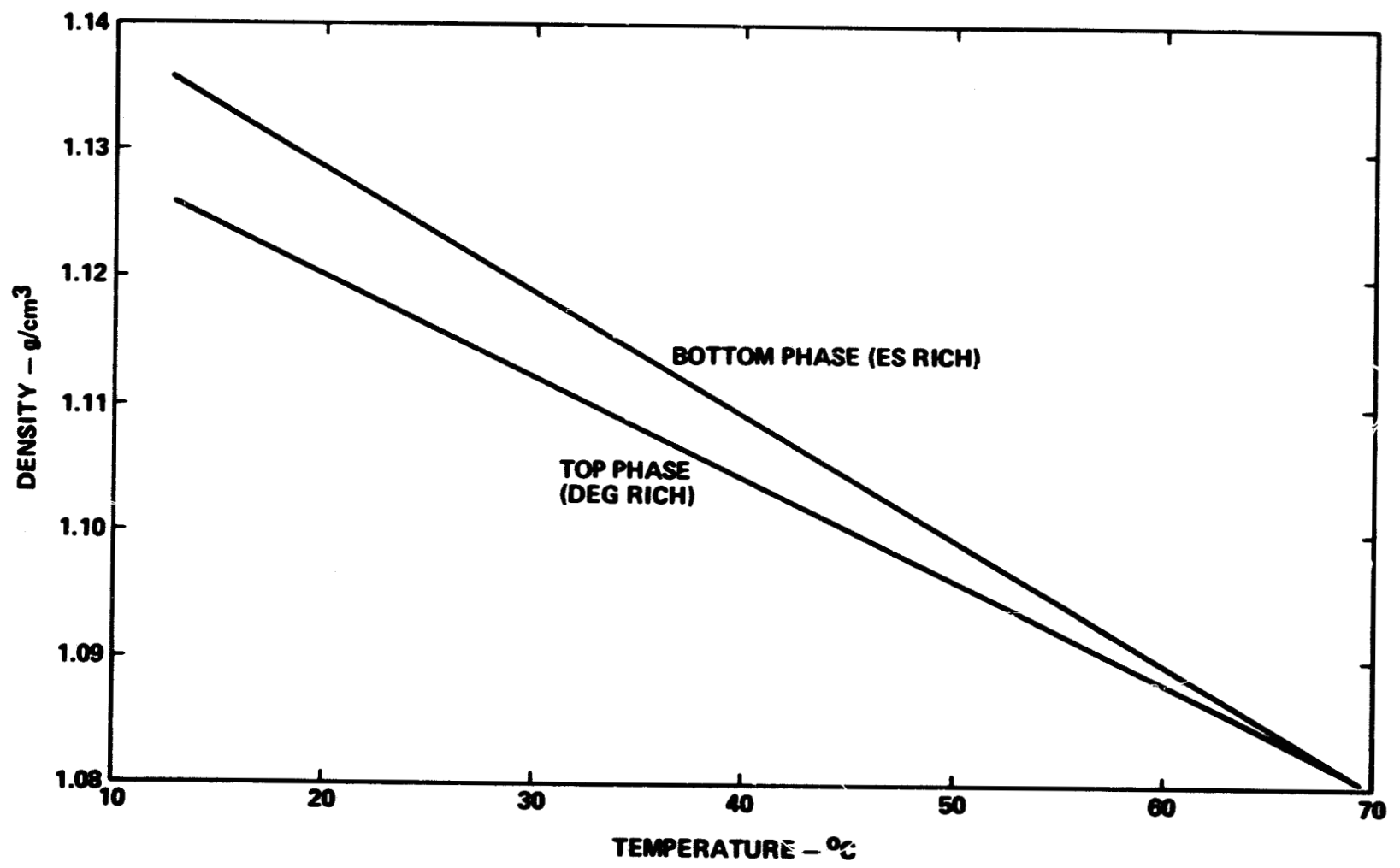


Figure 4. Density versus temperature for saturated phases, ES/DEG.

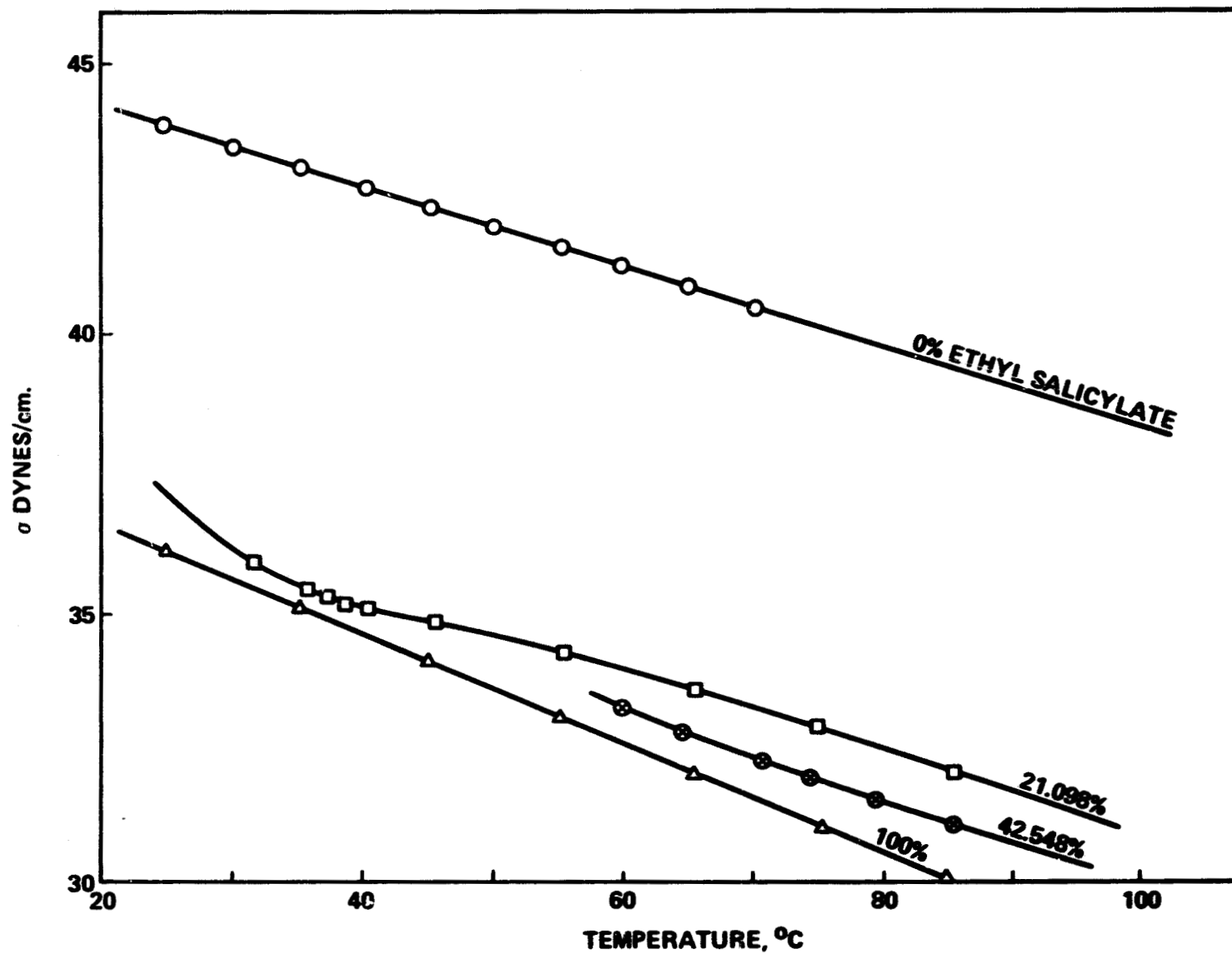
ORIGINAL PAGE IS
OF POOR QUALITY

Figure 5. Surface tension (σ) versus temperature, various compositions of ethyl salicylate-diethylene glycol.

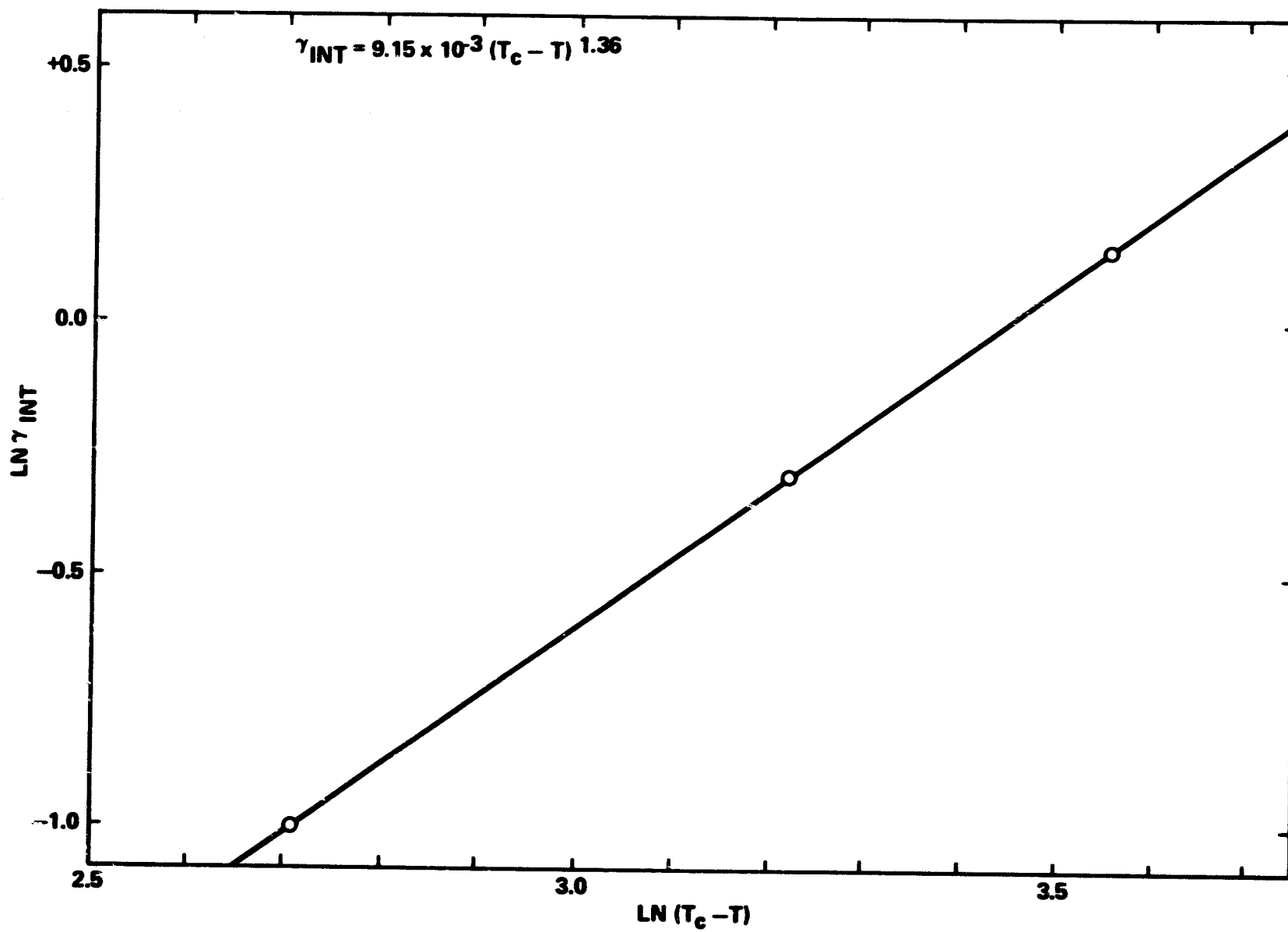


Figure 6. $\text{LN } \gamma_{\text{INT}}$ versus $\text{LN}(T_c - T)$ for ethyl salicylate-diethylene glycol.

ORIGINAL PAGE IS
OF POOR QUALITY

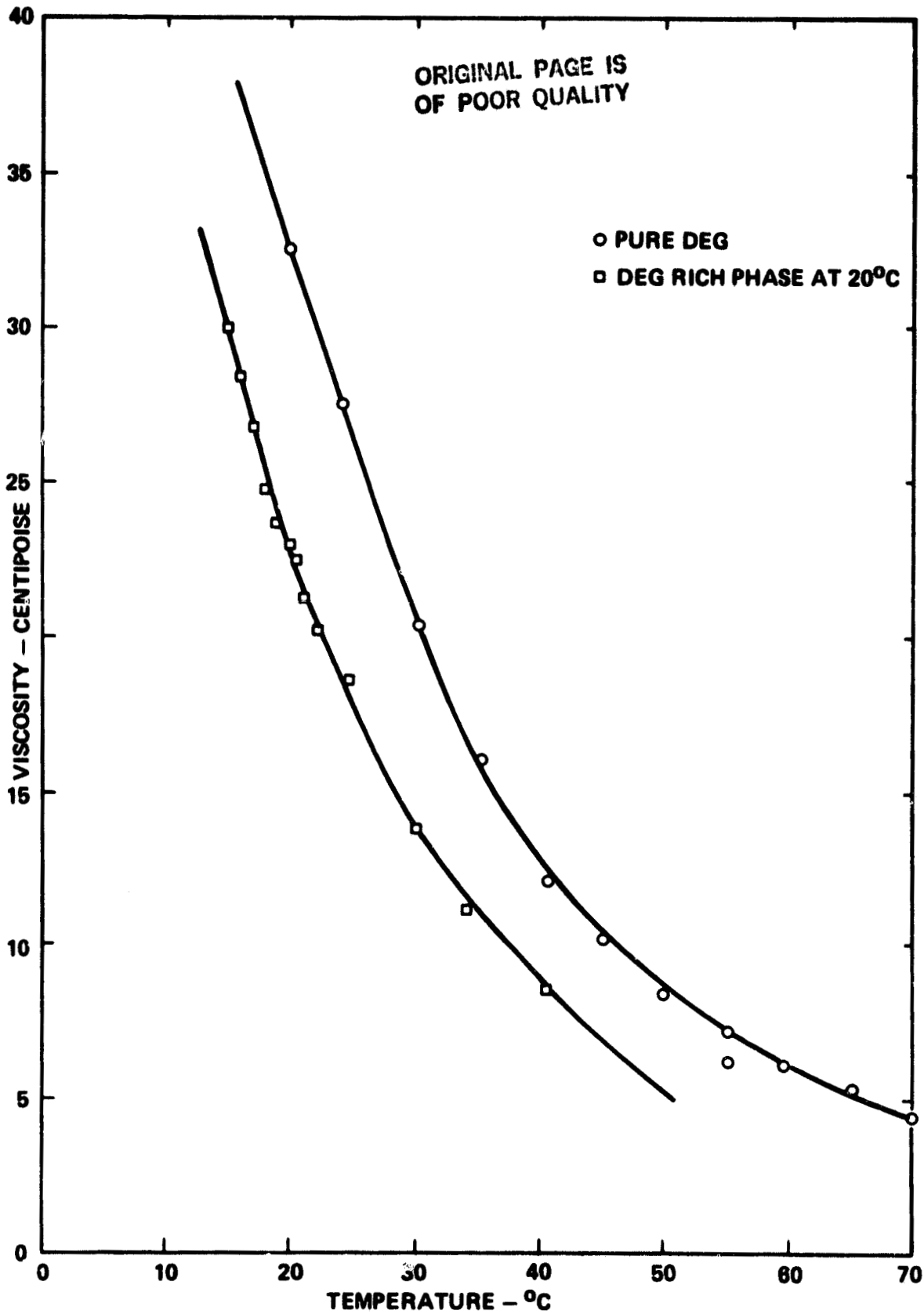


Figure 7. Viscosity versus temperature for DEG and DEG-rich phase (saturated at 20°C).

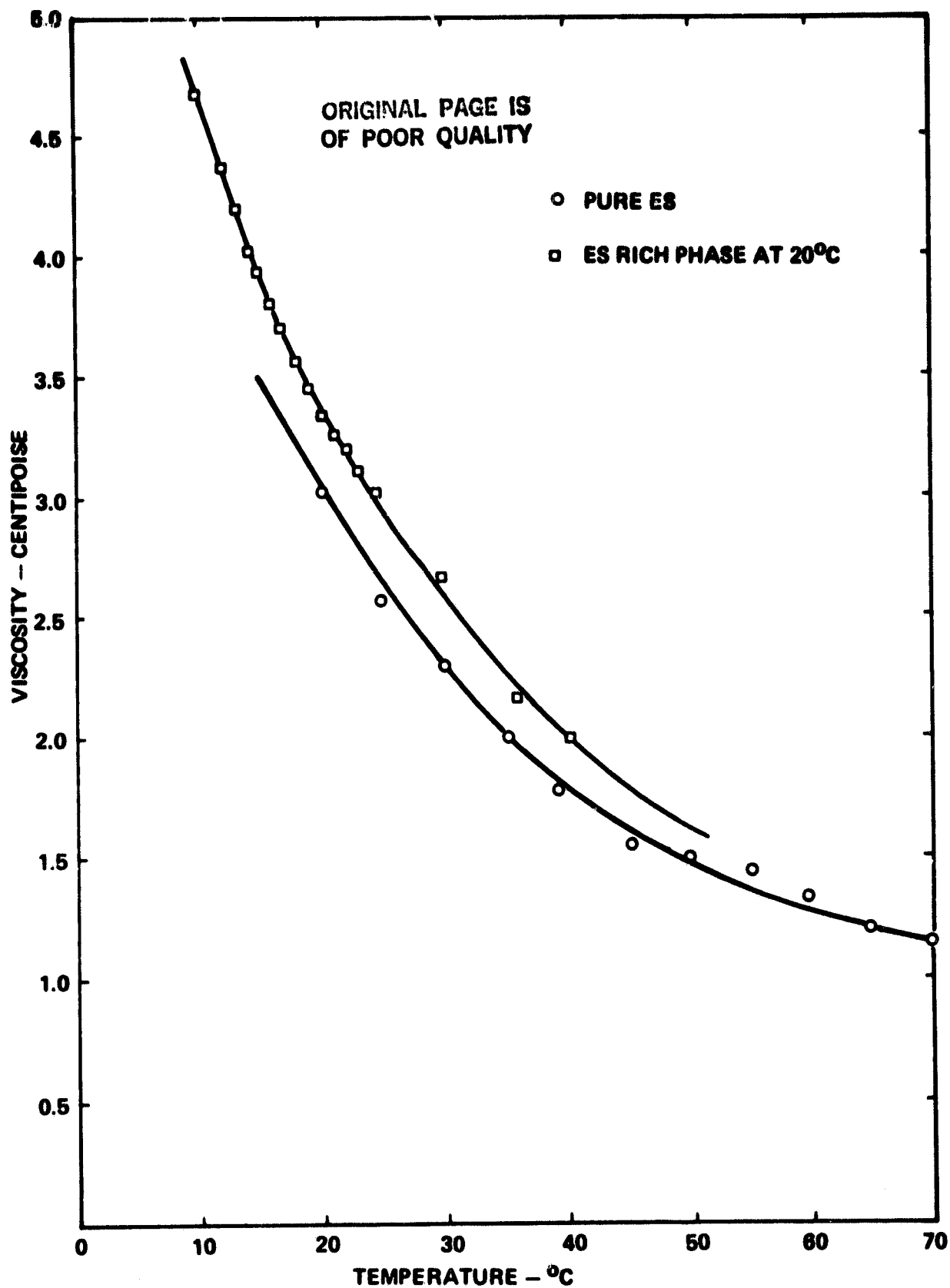


Figure 8. Viscosity versus temperature for ES and ES-rich phase (saturated at 20°C).

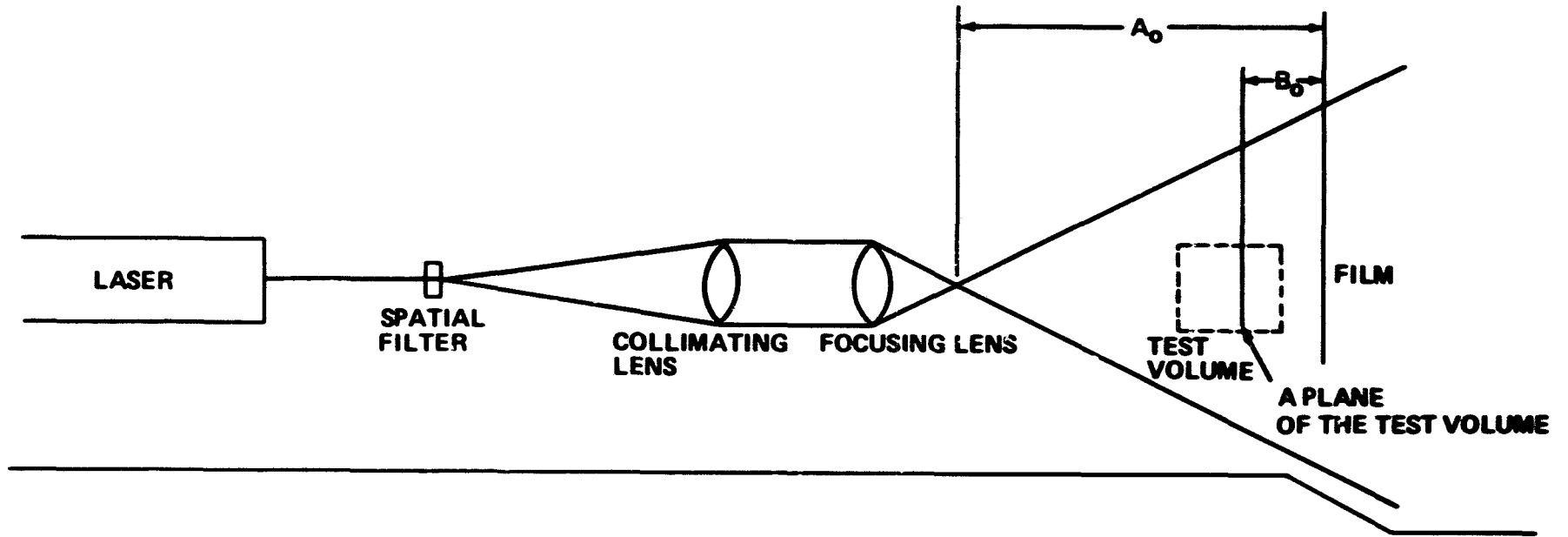


Figure 9. Construction system.

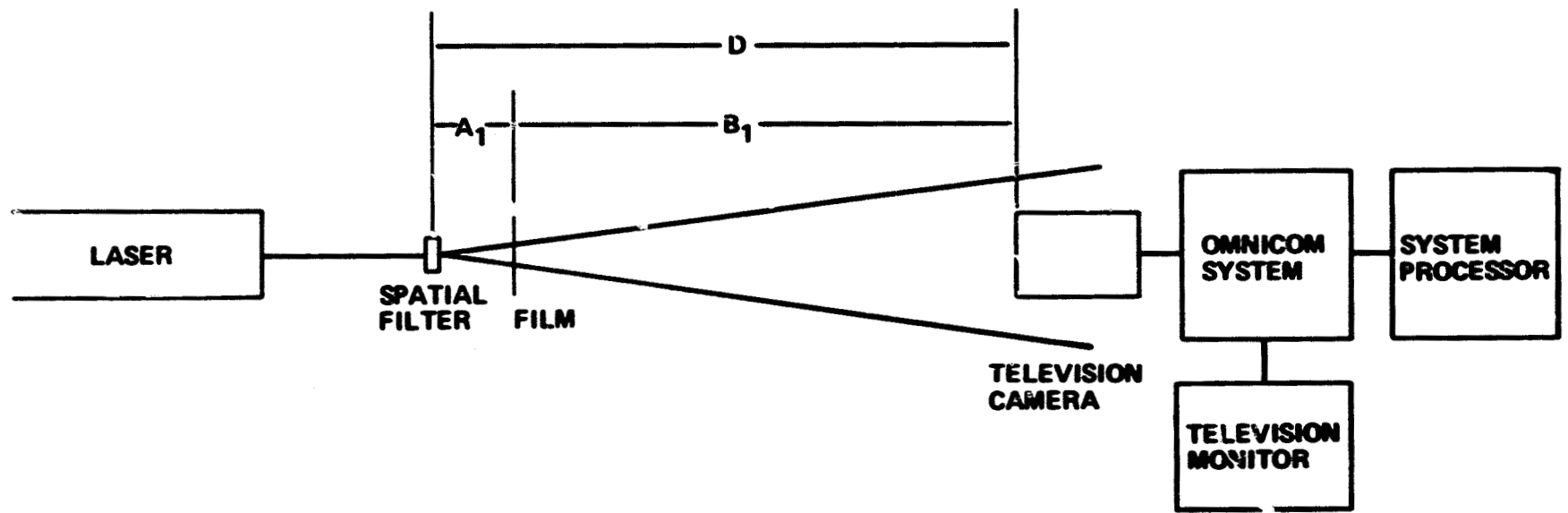
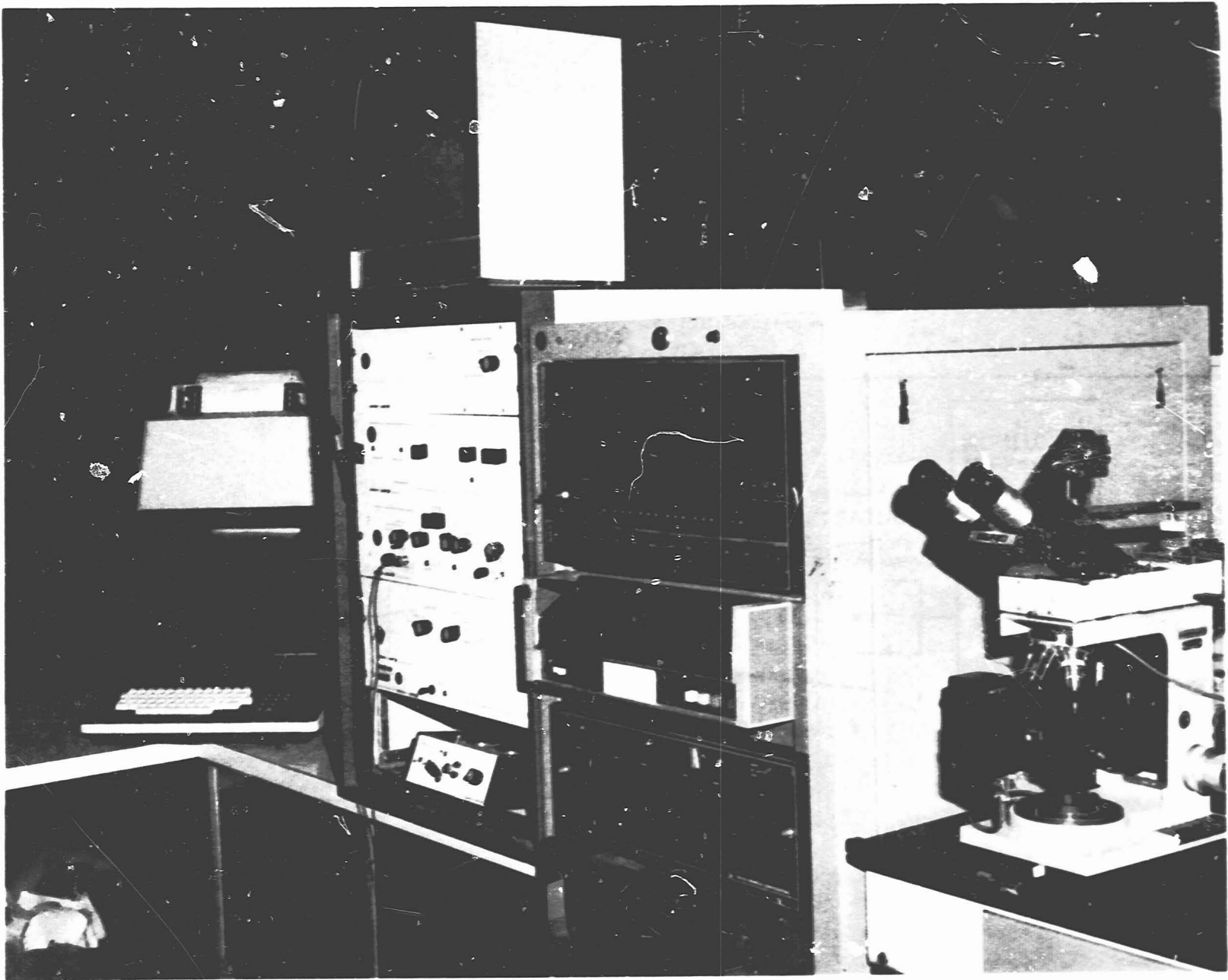


Figure 10. Reconstruction system.

ORIGINAL PAGE IS
OF POOR QUALITY



ORIGINAL PAGE
BLACK AND WHITE PHOTOGRAPH

Figure 11. Bausch and Lomb automated feature-analysis Omnicon system.

ORIGINAL PAGE IS
OF POOR QUALITY

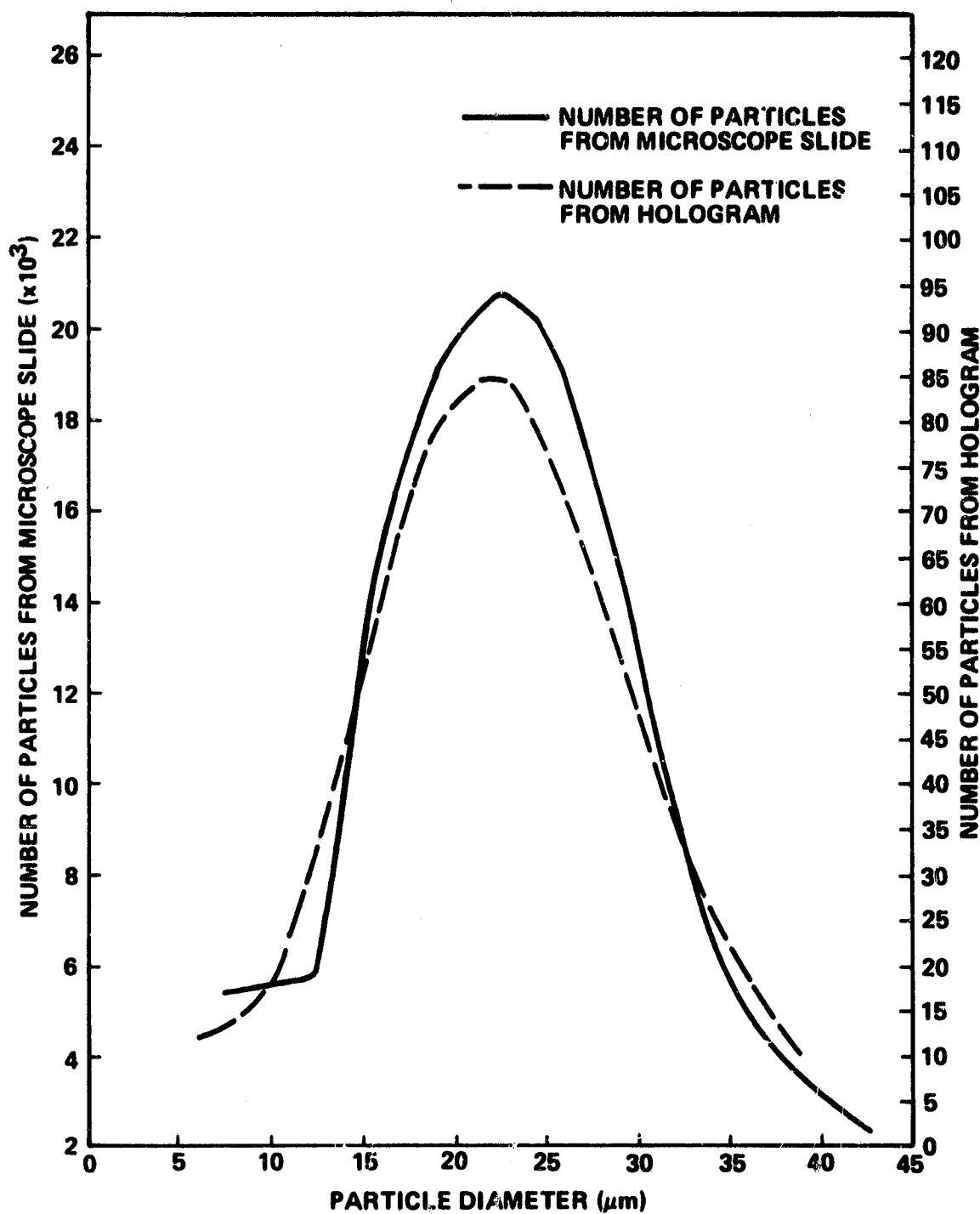


Figure 12. Comparison of particle dispersions measured by the Omnicon system from normal microscopy techniques and holographic microscope techniques.

ORIGINAL PAGE IS
OF POOR QUALITY

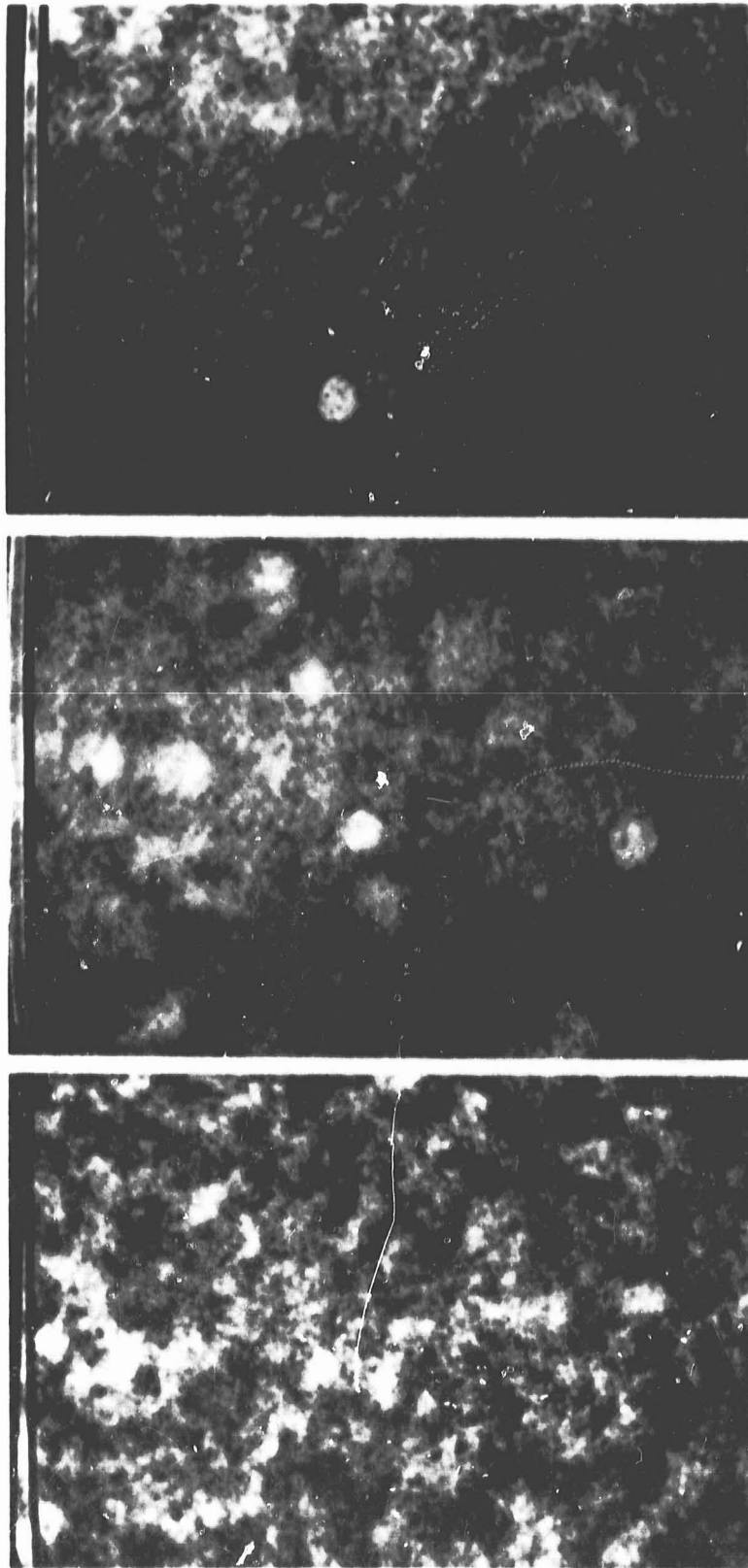
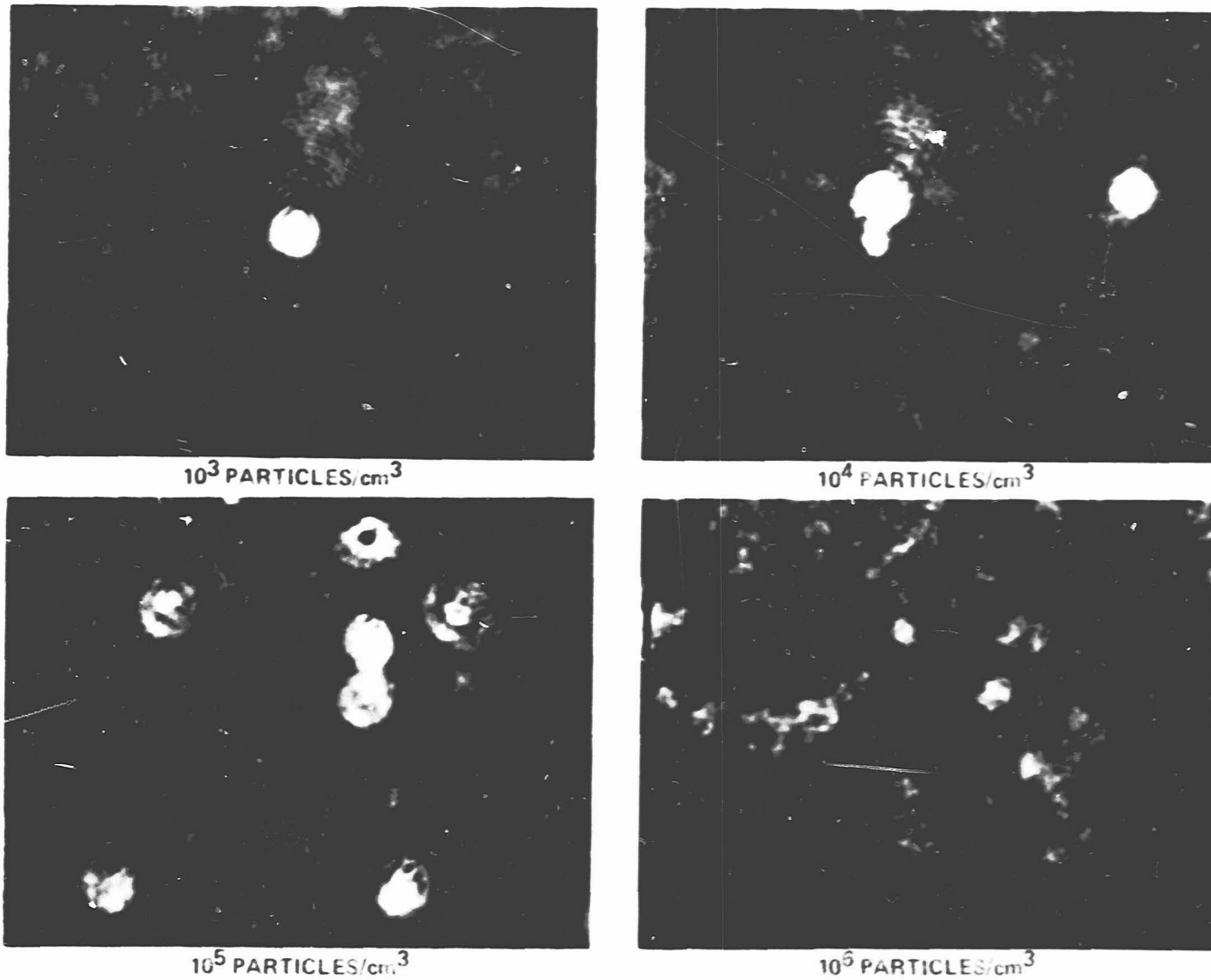


Figure 13. Different particle densities: 10^3 (top), 10^4 (center),
and 10^5 (bottom) particles/cm³.

HOLOGRAPHIC MICROSCOPY

HIGHER PARTICLE DENSITIES CAN BE RECORDED HOLOGRAPHICALLY WITH CORRESPONDING DECREASES IN THE OPTICAL PATH LENGTH OF THE TEST CELL. THE TEST CELL PATH LENGTH IN THESE PHOTOGRAPHS WAS 1mm.



ORIGINAL PAGE IS
OF POOR QUALITY

Figure 14. Different particle densities in a 1-mm pathlength test cell.

ORIGINAL PAGE IS
OF POOR QUALITY

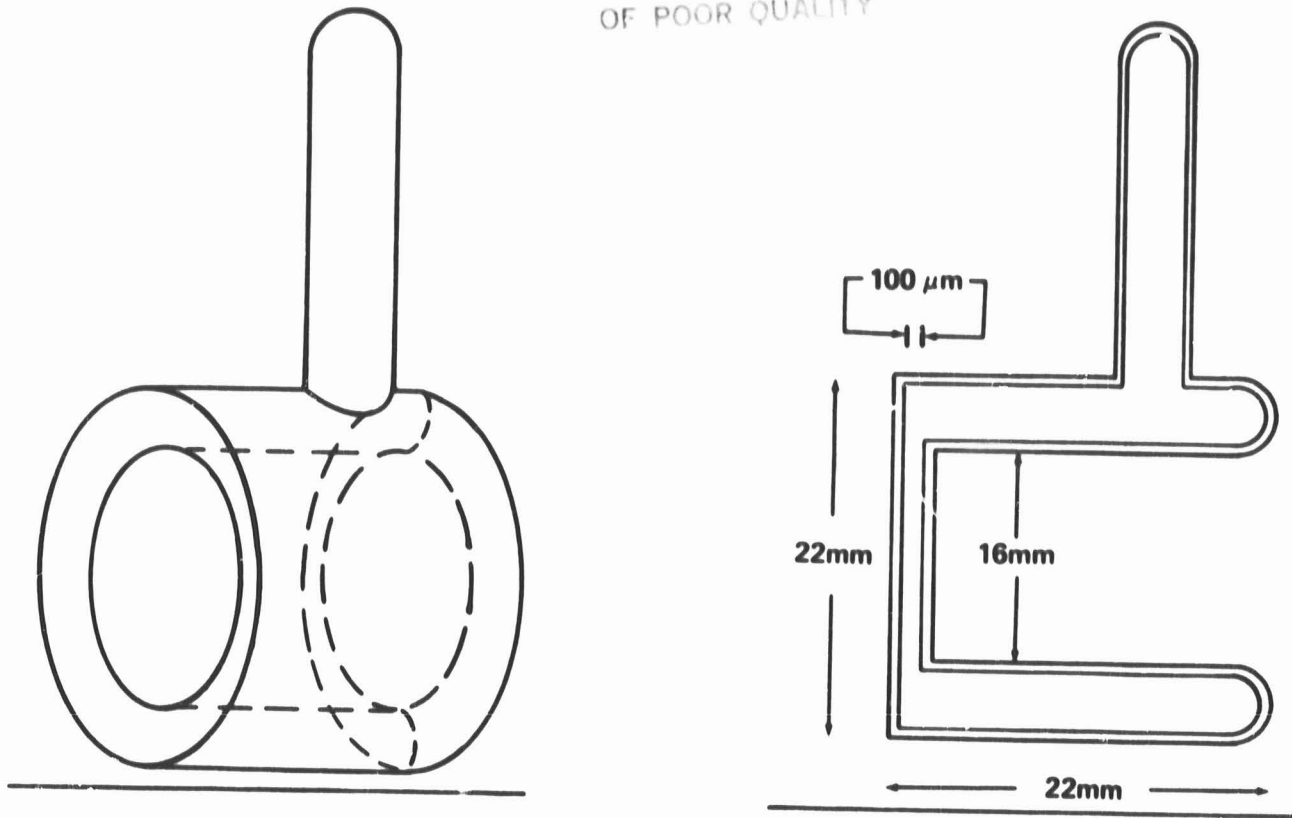


Figure 15. Test cell.

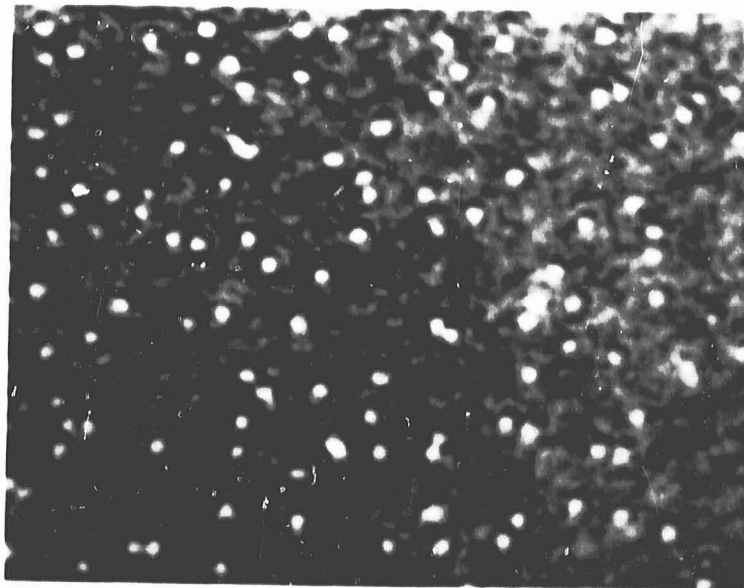
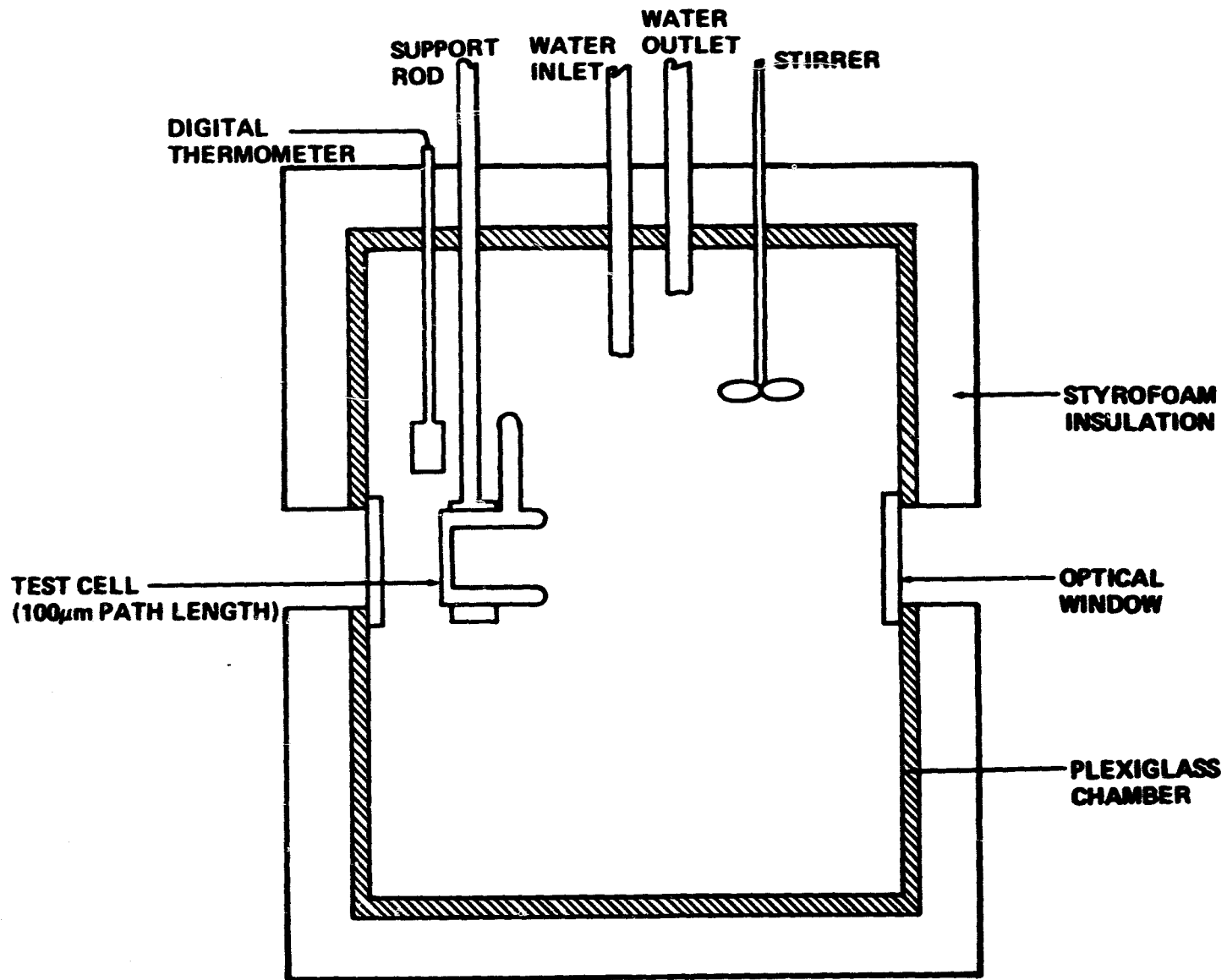


Figure 16. 10^7 particles/cm³ in a 100-μm pathlength test cell.



ORIGINAL PAGE IS
OF POOR QUALITY

Figure 17. Holographic isothermal test chamber.

ORIGINAL PAGE IS
OF POOR QUALITY

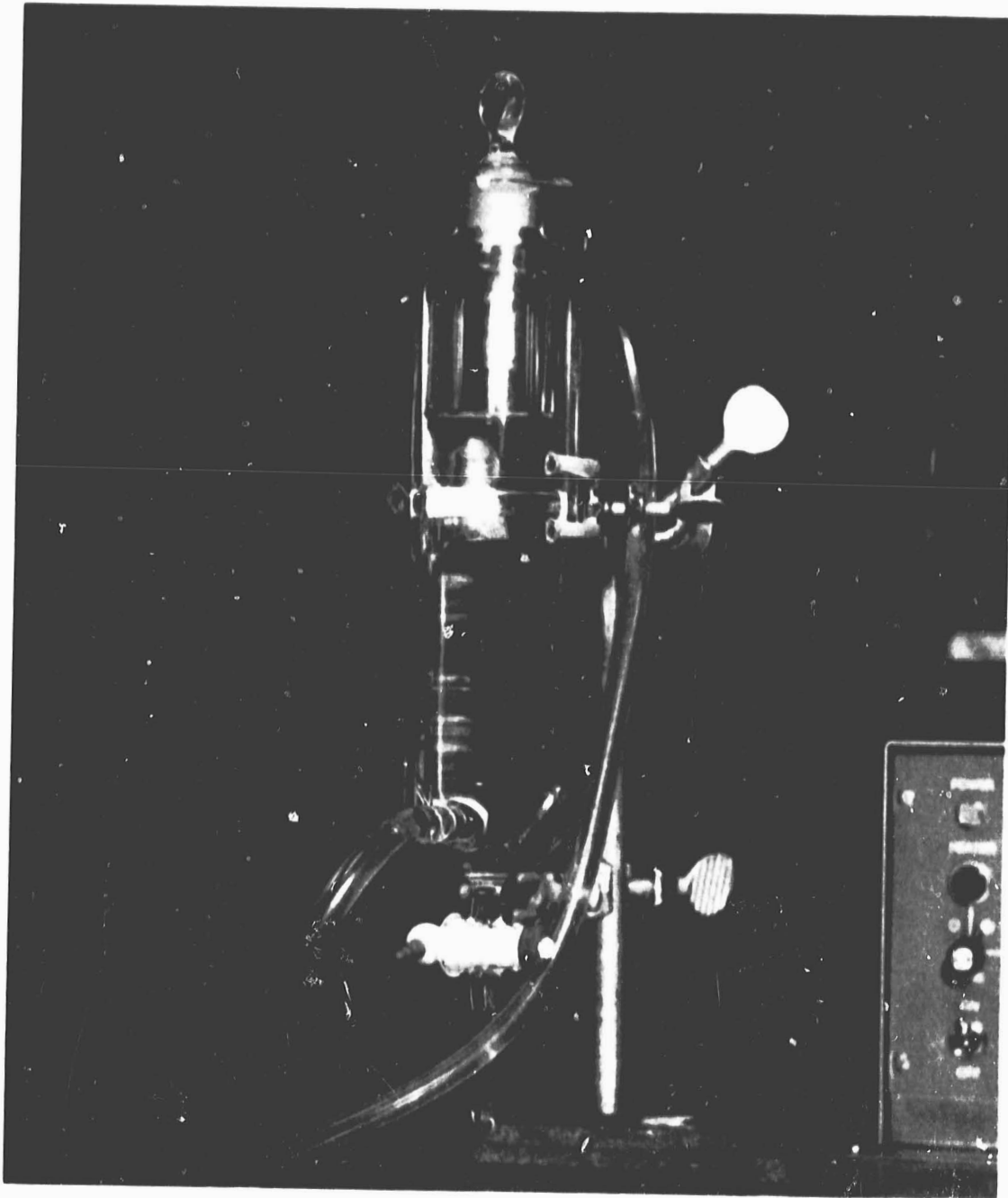
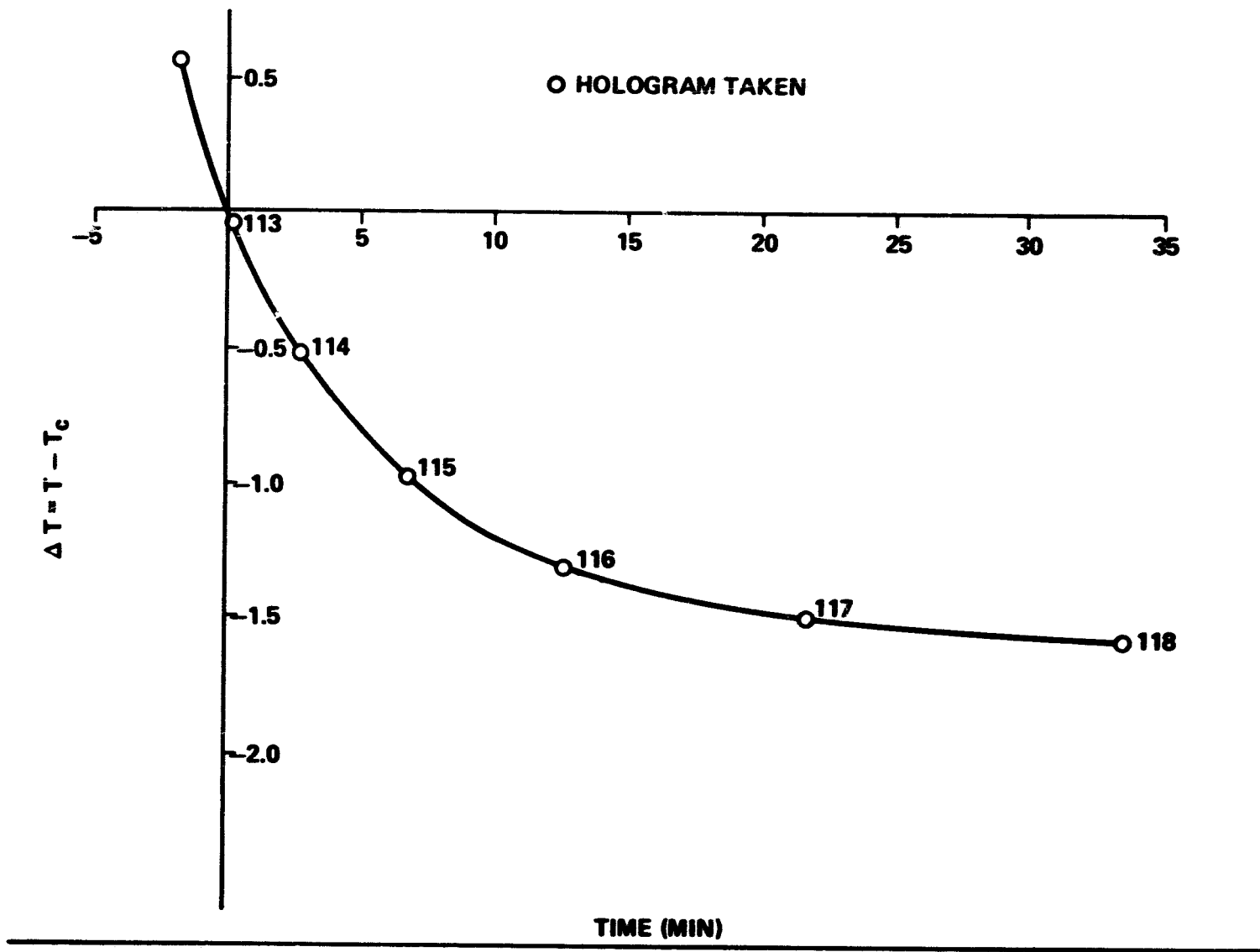


Figure 18. Isothermal phase equilibration chamber.



ORIGINAL PAGE IS
OF POOR QUALITY

Figure 19. Thermal history and holographic exposures for ES/DEG experiment.

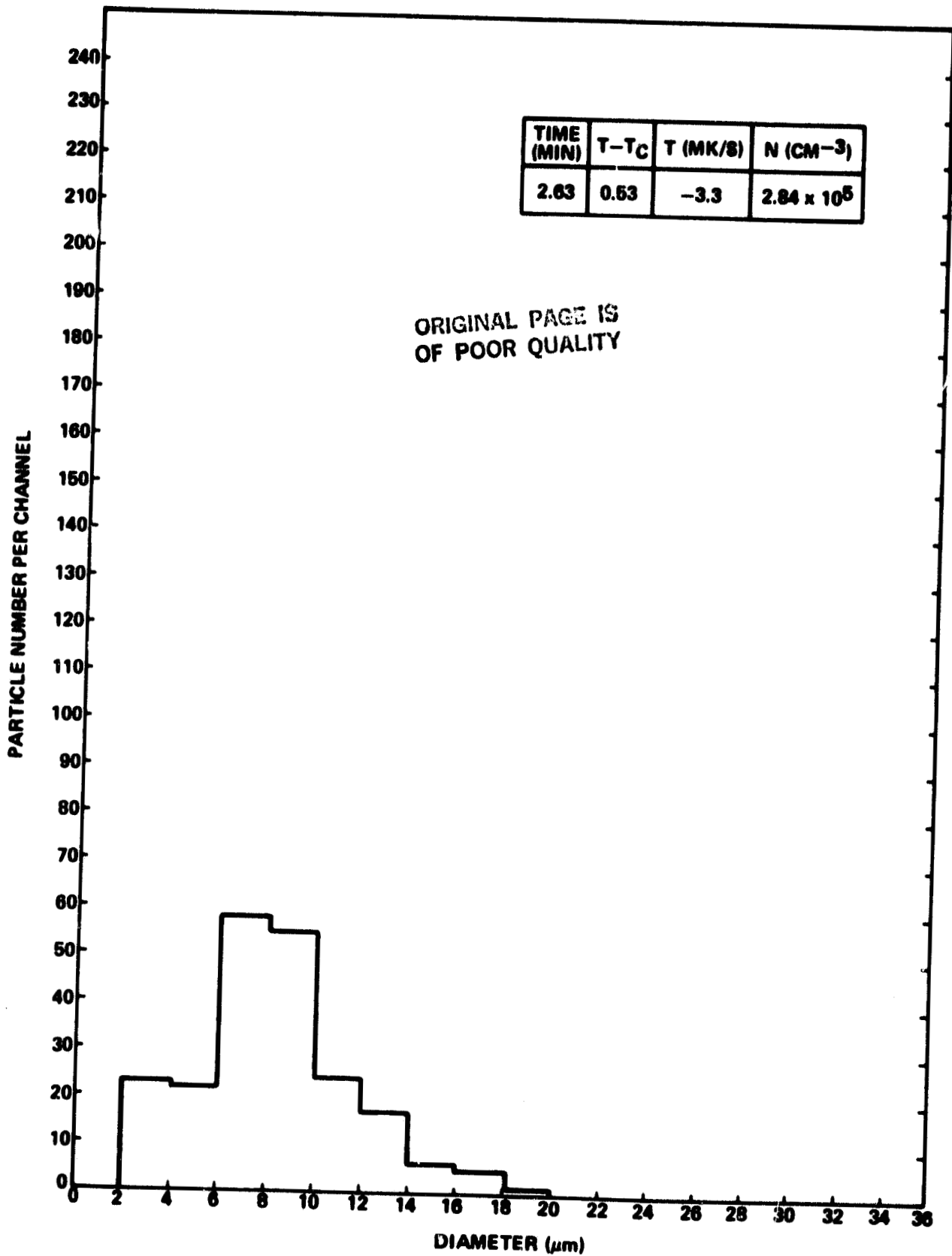


Figure 20a. Particle size distribution; hologram No. 114.

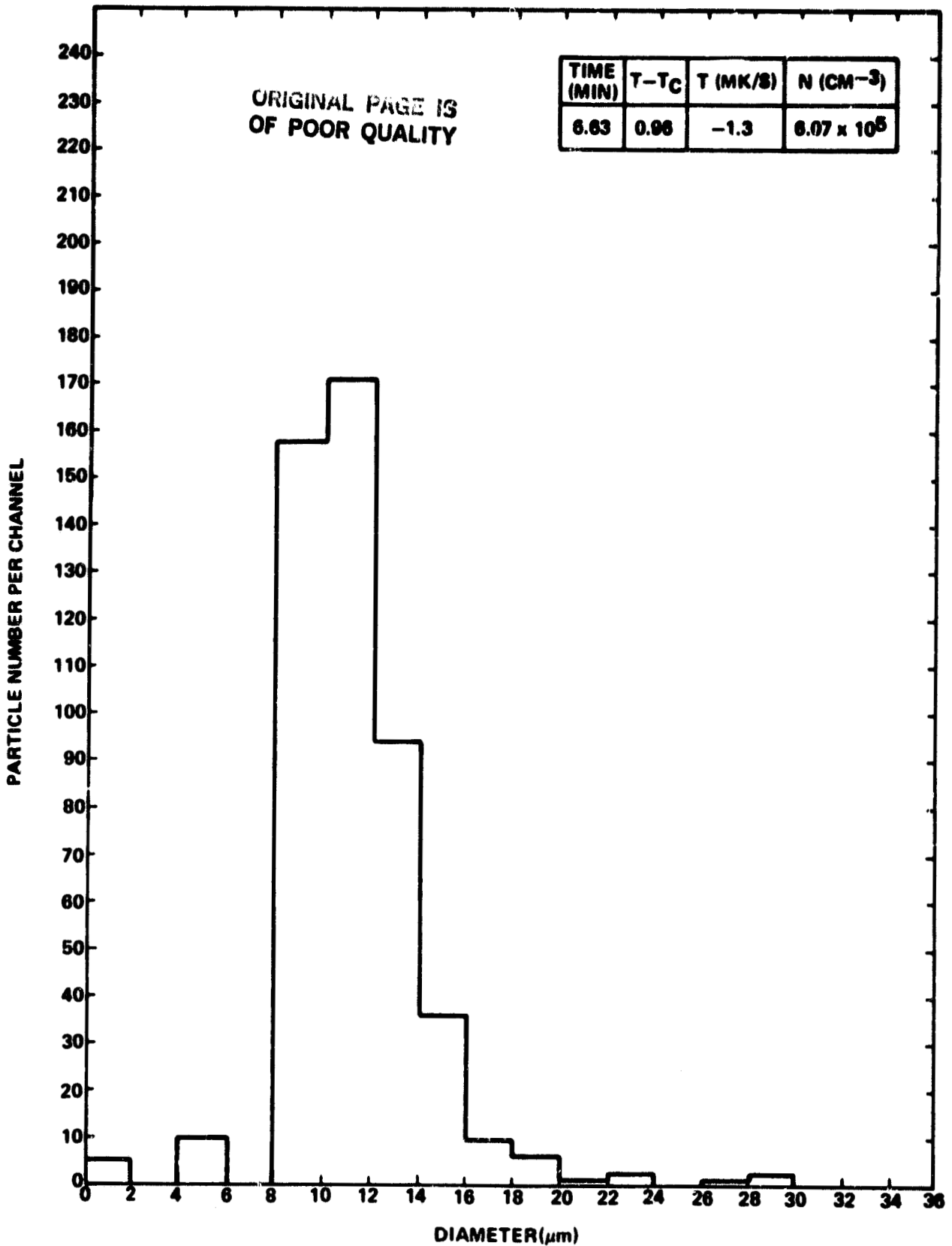


Figure 20b. Particle size distribution; hologram No. 115.

ORIGINAL PAGE IS
OF POOR QUALITY

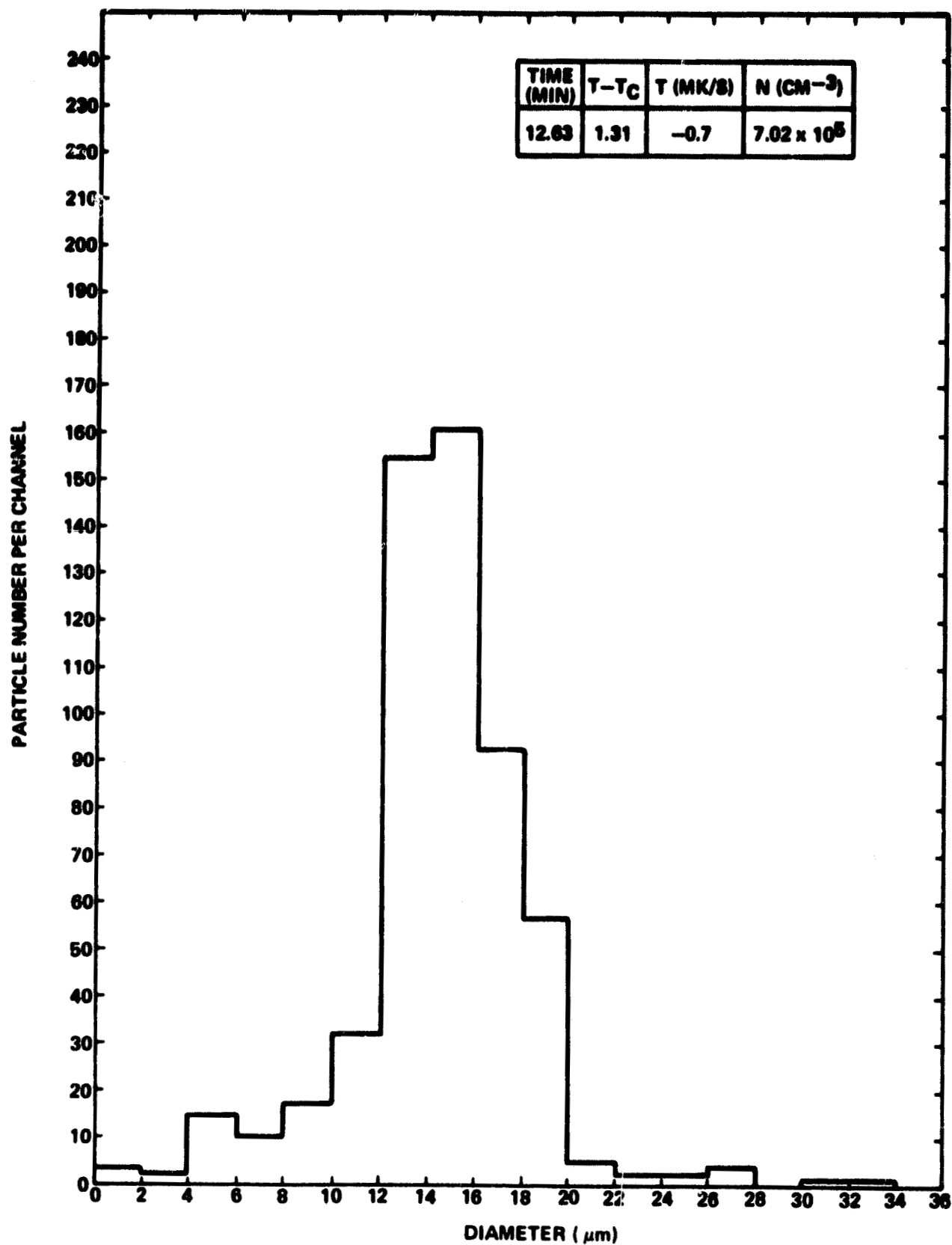


Figure 20c. Particle size distribution; hologram No. 116.

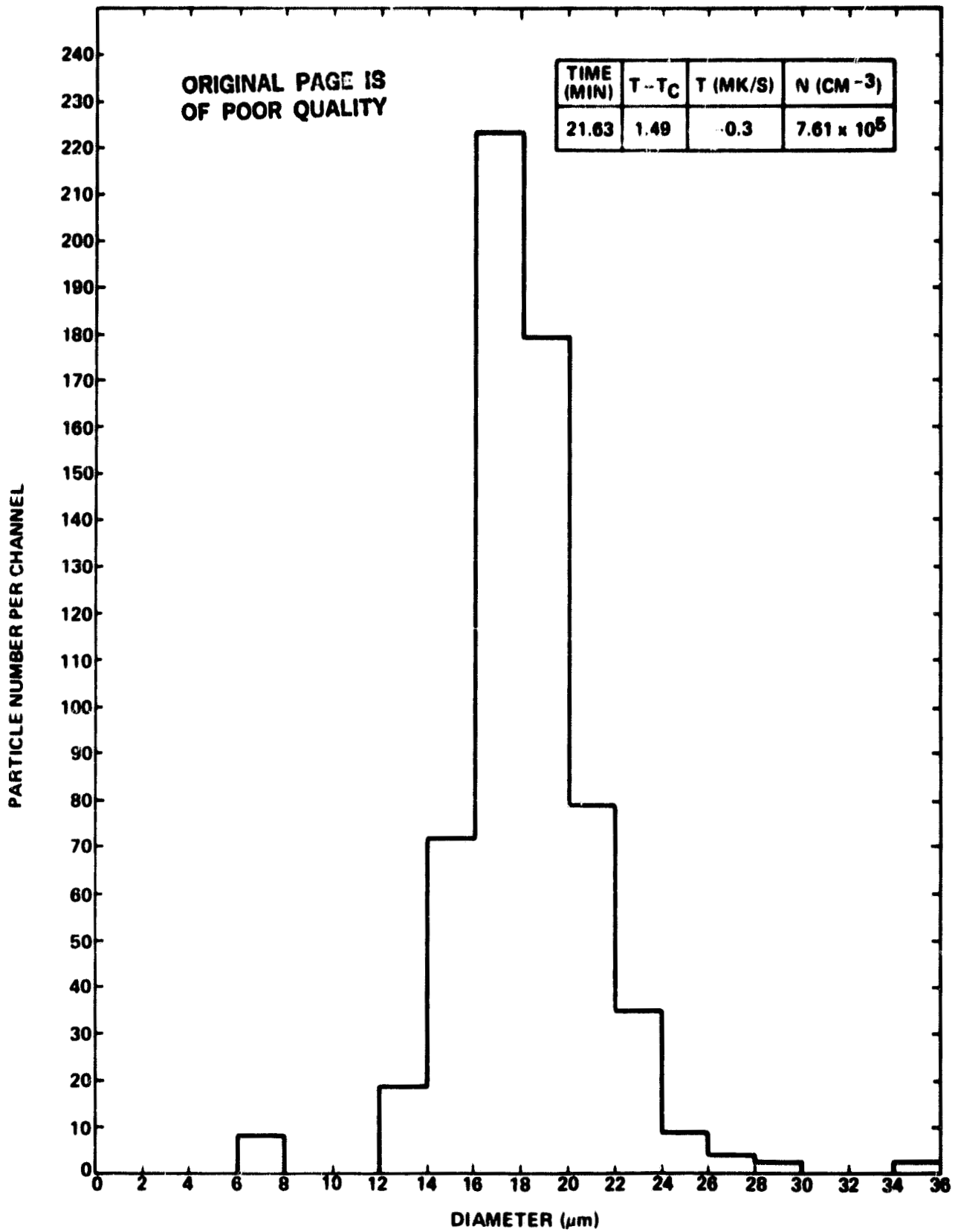


Figure 20d. Particle size distribution, hologram No. 117.

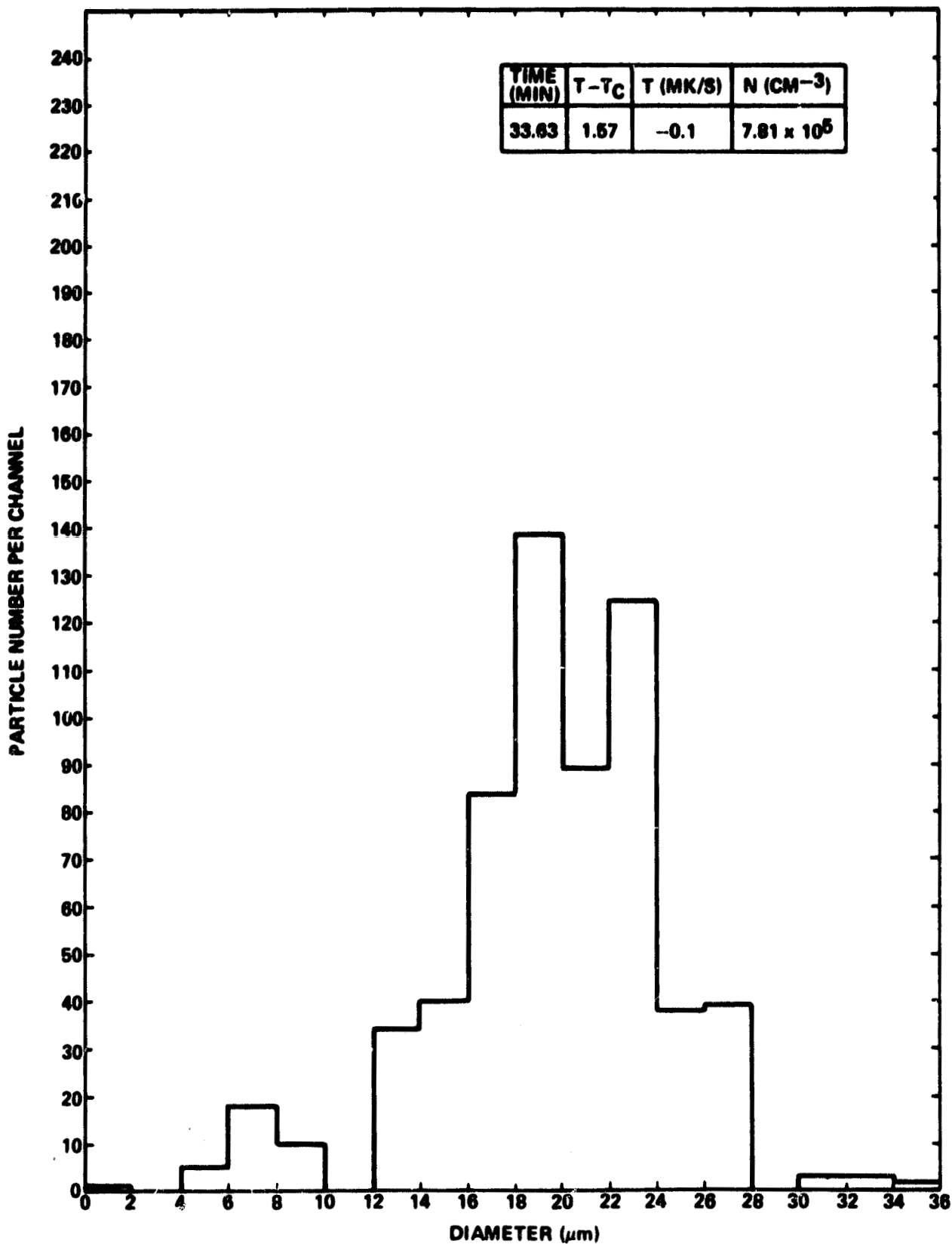
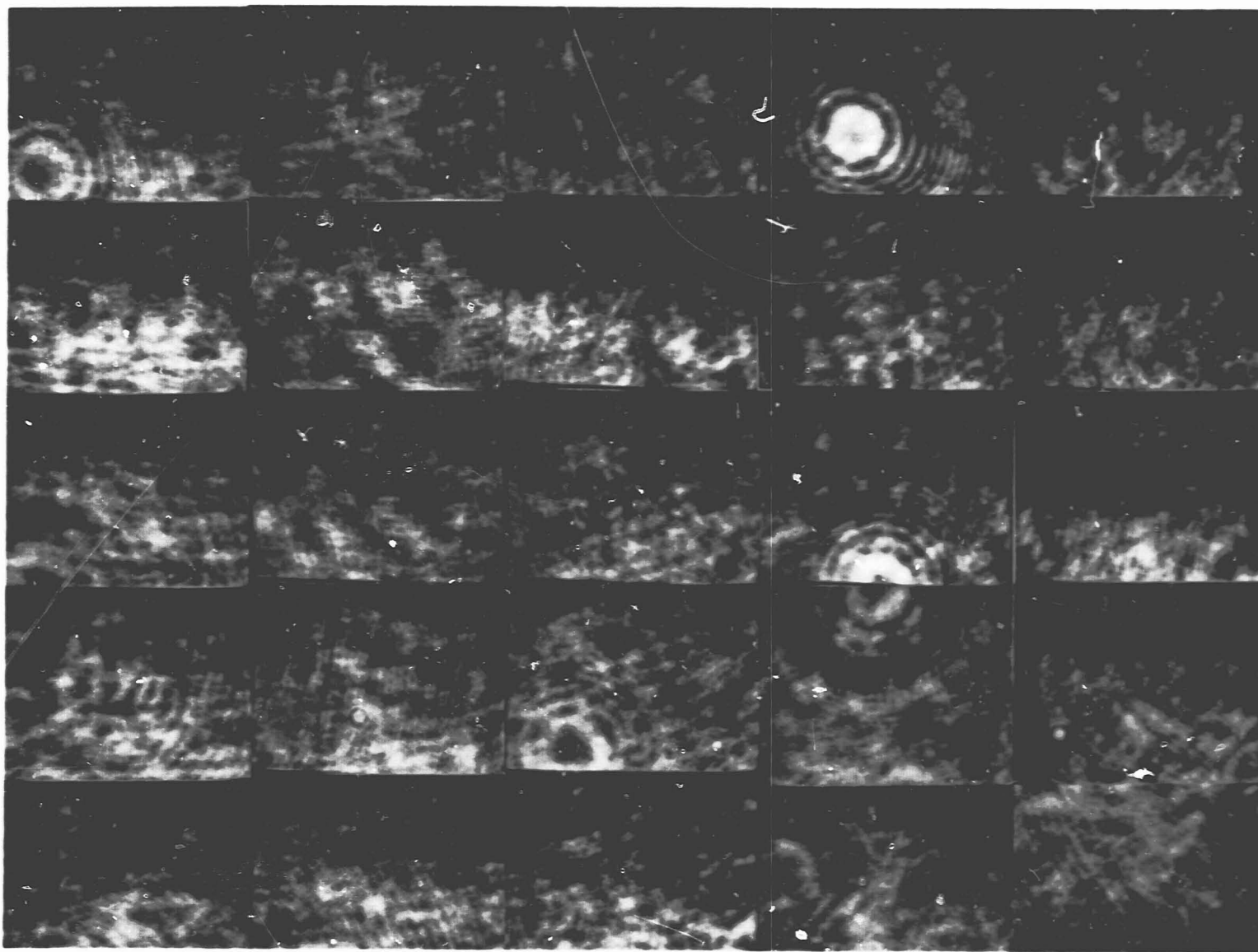


Figure 20e. Particle size distribution, hologram No. 118.



ORIGINAL PAGE IS
OF POOR QUALITY

Figure 21a. Series of composite photographs taken from holograms at a magnification of 62X showing growth of the separating (ES rich) phase.

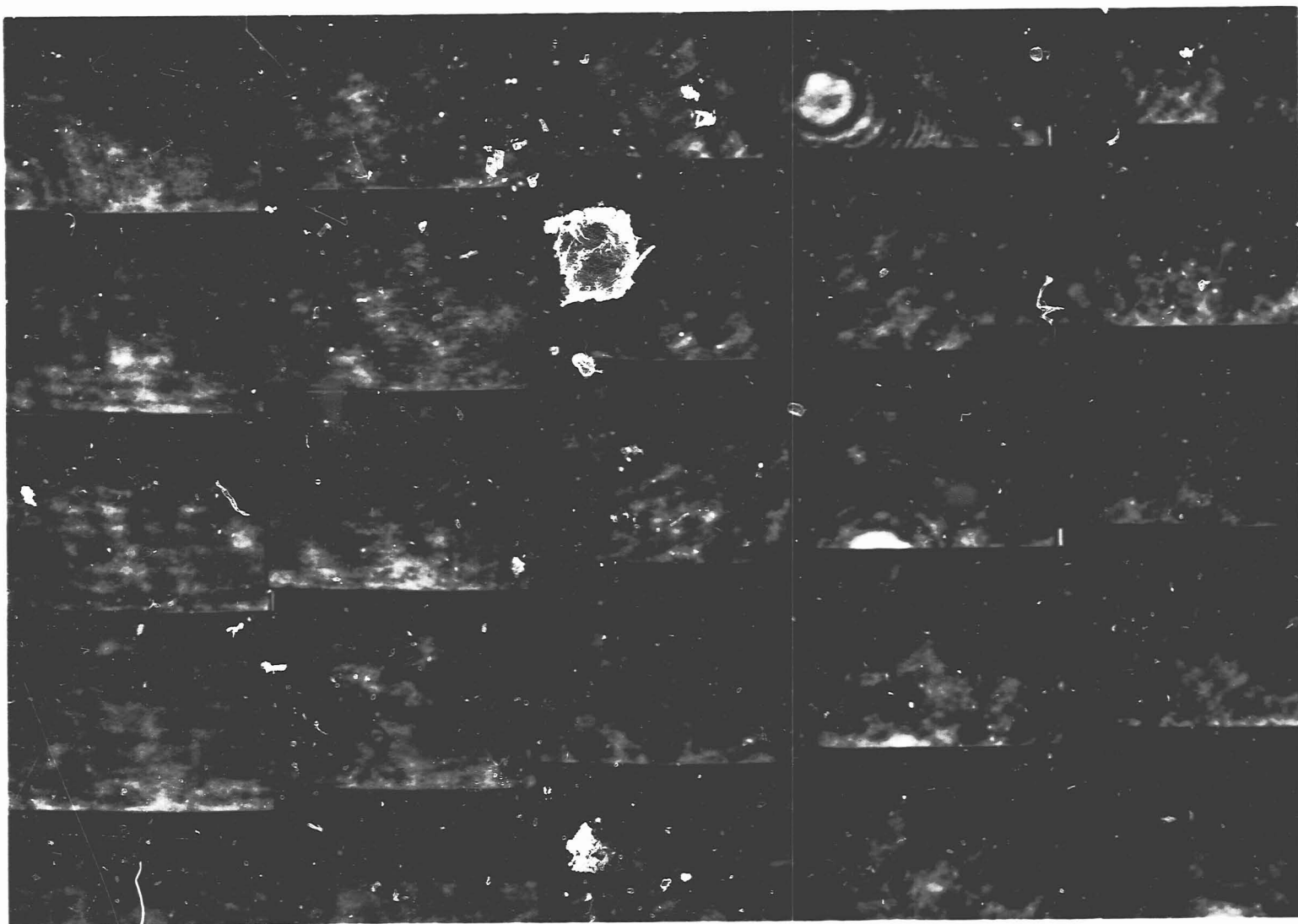
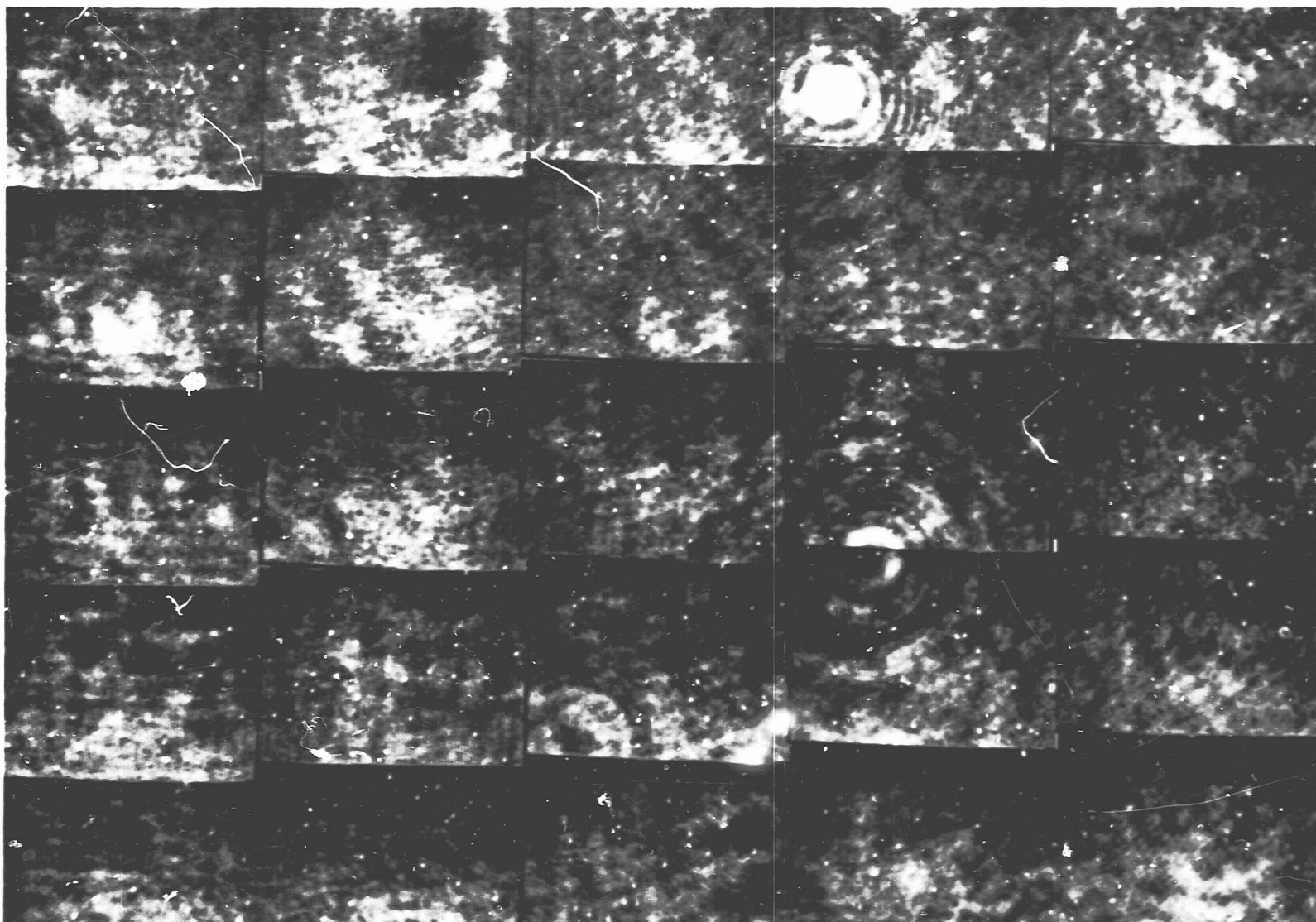


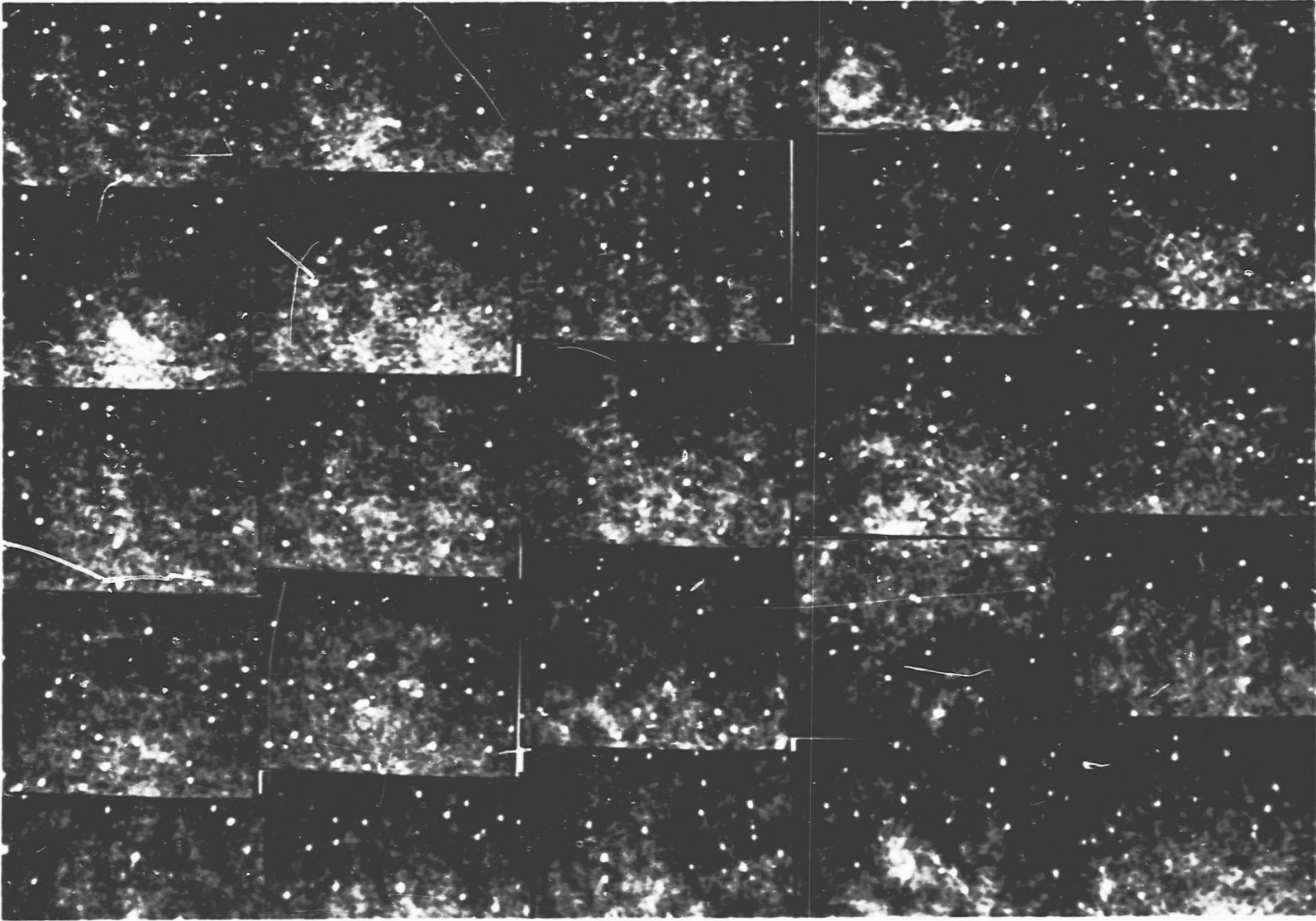
Figure 21b. Hologram No. 114, $t = 157.8$ sec, $\Delta T = 0.53$ K.

ORIGINAL PAGE IS
OF POOR QUALITY



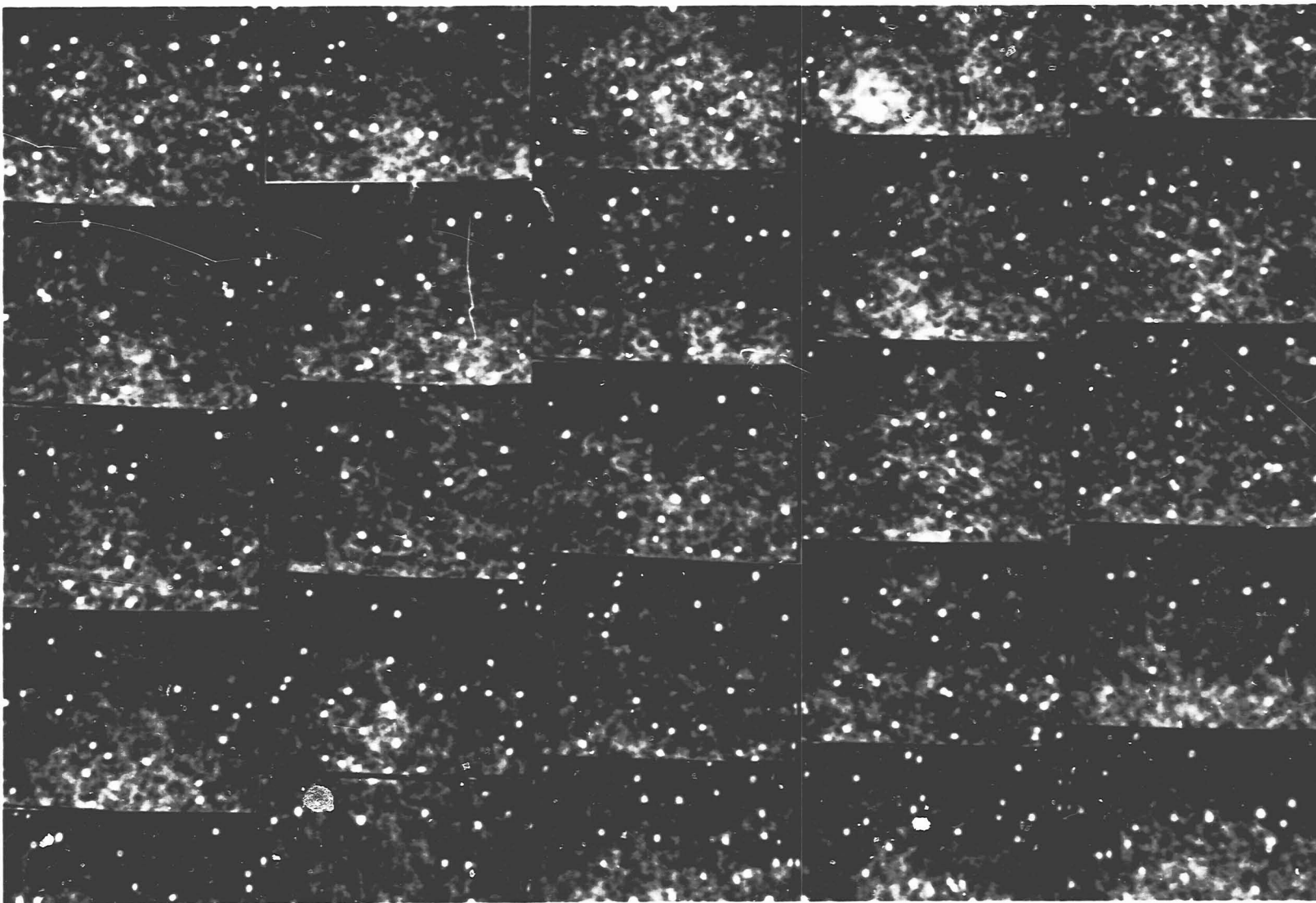
ORIGINAL PAGE IS
OF POOR QUALITY

Figure 21c. Hologram No. 115, $t = 397.8$ sec, $\Delta T = 0.96$ K.



ORIGINAL PAGE IS
OF POOR QUALITY

Figure 21d. Hologram No. 116, $t = 757.8$ sec, $\Delta T = 1.31$ K.



ORIGINAL PAGE IS
OF POOR QUALITY

Figure 21e. Hologram No. 117, $t = 1297.8$ sec, $\Delta T = 1.49$ K.

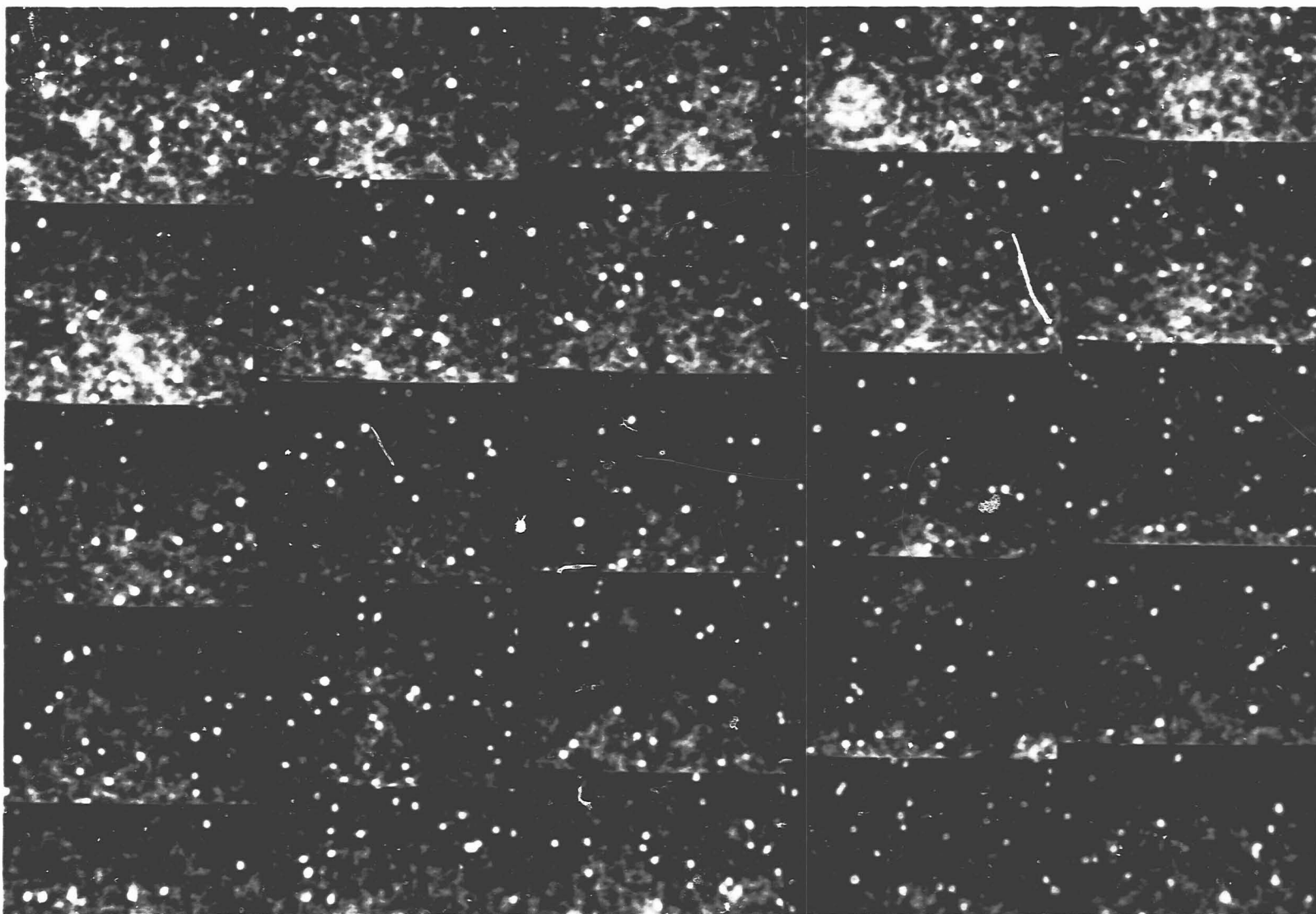


Figure 21f. Hologram No. 118, $t = 2017.8$ sec, $\Delta T = 1.57$ K.

ORIGINAL PAGE IS
OF POOR QUALITY

ORIGINAL PAGE 13
OF POOR QUALITY

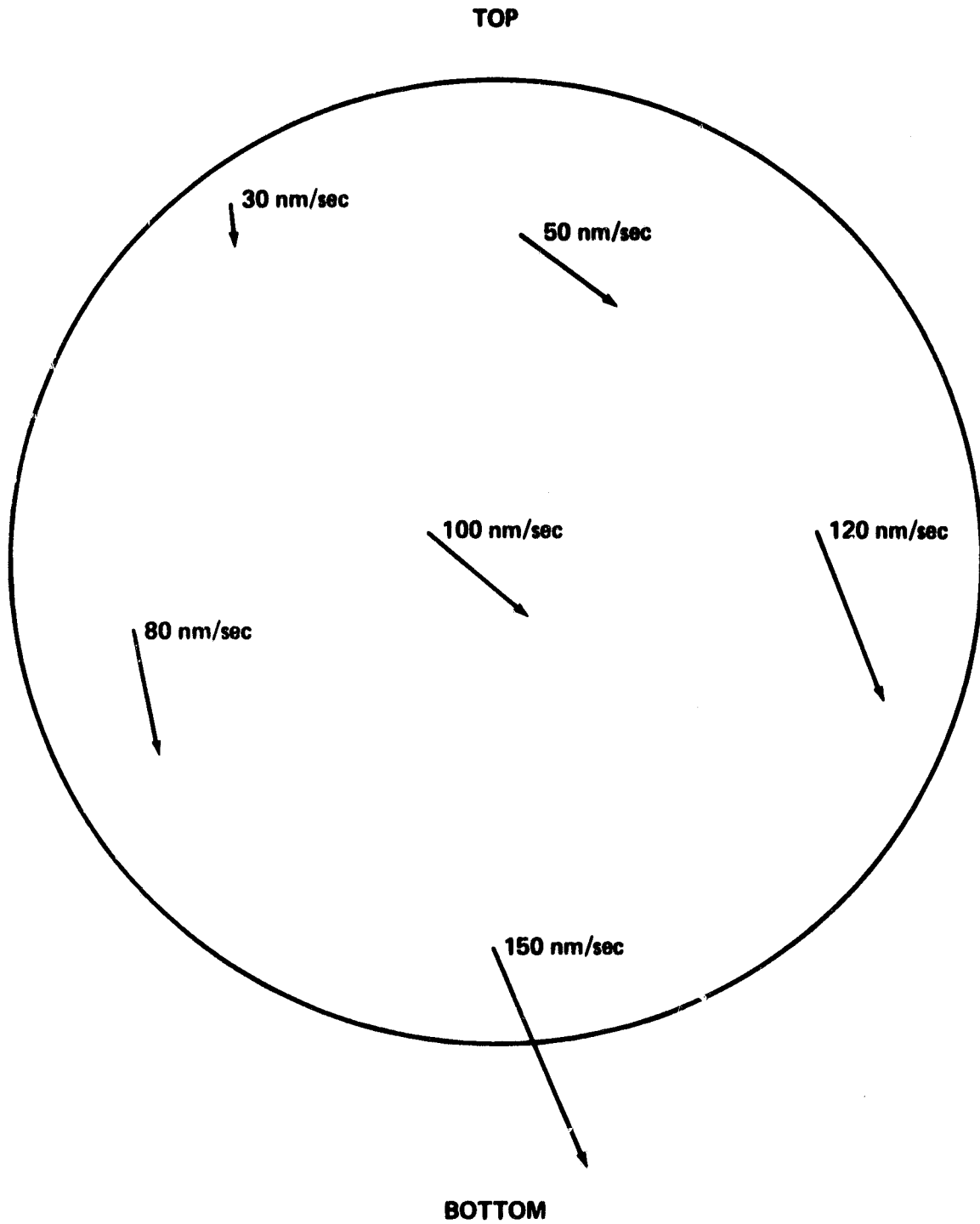


Figure 22. Measured particle motion in various parts of the test cell.

ORIGINAL PAGE IS
OF POOR QUALITY

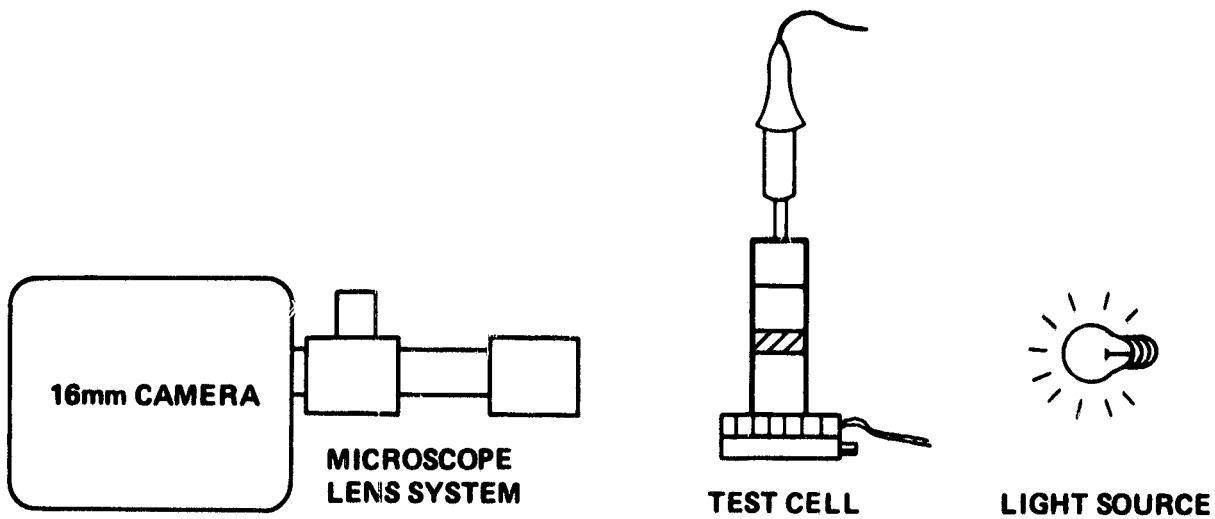
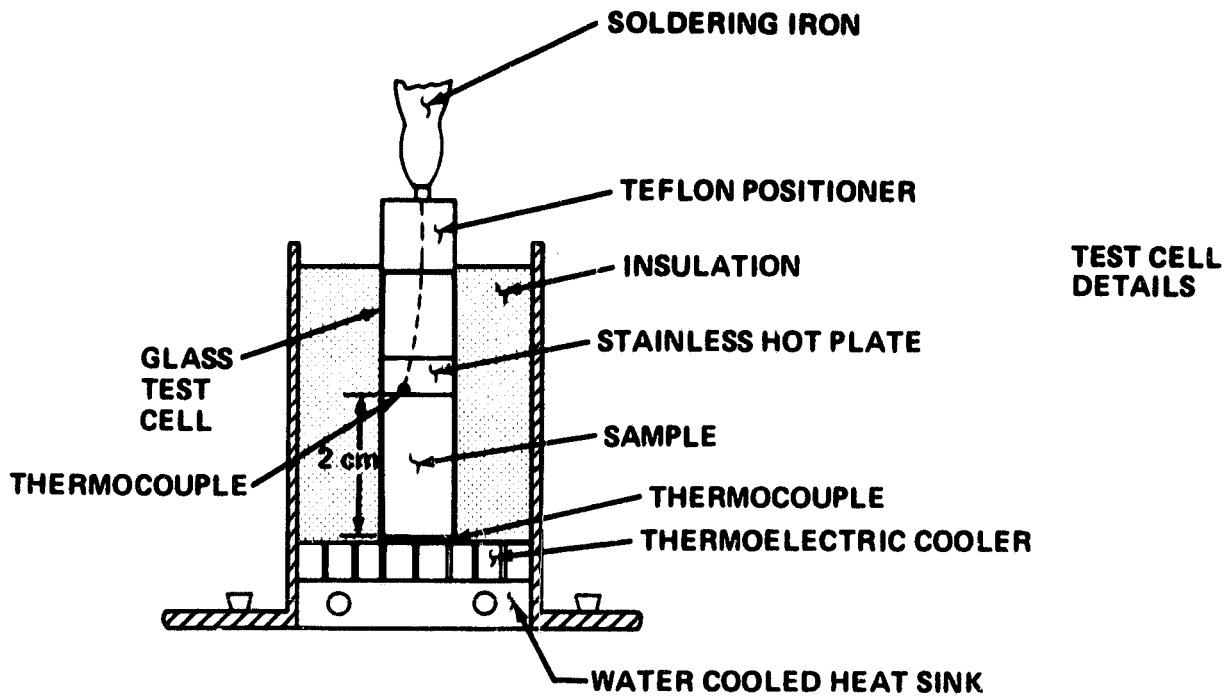
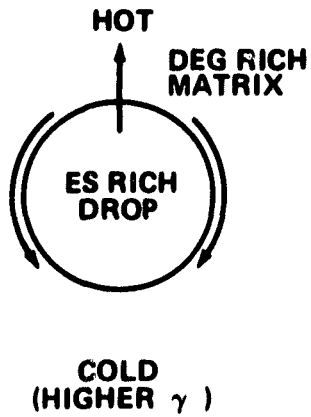


Figure 23. Schematic of immiscible fluid thermal migration apparatus.

ORIGINAL PAGE IS
OF POOR QUALITY

EFFECT OF TEMPERATURE



EFFECT OF CONCENTRATION

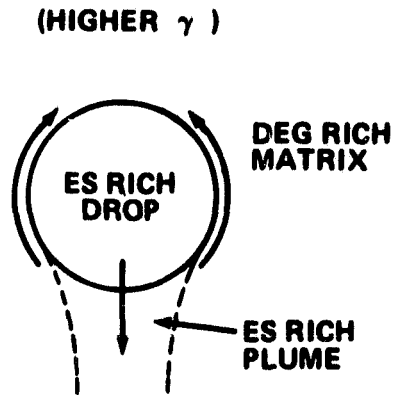


Figure 24. Relative effects of thermal and concentration gradients on interfacial tension driven droplet motion.

TABLE 1. DENSITIES OF ETHYL SALICYLATE-DIETHYLENE
GLYCOL SOLUTIONS

(a) Density of Homogeneous Solutions		
Mole % ES	Temperature (°C)	Density (g/cm ³)
0.0	26.50	1.1150
0.0	32.60	1.1109
0.0	41.25	1.1048
0.0	50.81	1.0980
0.0	60.92	1.0907
0.0	70.20	1.0839
0.0	80.70	1.0754
6.614	30.23	1.1123
6.614	42.59	1.1037
6.614	50.79	1.0973
6.614	61.46	1.0895
6.614	70.19	1.0820
6.614	79.59	1.0752
24.440	50.52	1.0973
24.440	60.11	1.0899
24.440	69.72	1.0823
24.440	80.25	1.0740
36.712	68.50	1.0838
36.712	73.85	1.0793
36.712	85.72	1.0696
69.844	69.82	1.0827
69.844	80.32	1.0727
79.578	61.14	1.0913
79.578	70.43	1.0823
79.578	80.29	1.0732
93.465	41.93	1.1114
93.465	51.20	1.1024
93.465	60.50	1.0934
93.465	70.45	1.0833
93.465	80.38	1.0733
100.0	29.80	1.1235
100.0	40.05	1.1147
100.0	51.24	1.1038
100.0	61.00	1.0942
100.0	70.22	1.0853
100.0	80.11	1.0759

(b) Density of Saturated Phases		
Temperature (°C)	Density (g/cm ³)	
	Top Layer	Bottom Layer
15.00	--	1.1316
25.00	1.1160	1.1260
35.00	1.1084	1.1160
45.00	1.1015	1.1020
55.00	1.0926	1.0938

TABLE 2. COMPARISON OF MEASURED AND CALCULATED VELOCITIES FOR SELECTED DROPS

dT/dx (°C/cm)	Drop Radius (μm)	Measured Velocity V _m (cm/sec)	Calculated Velocity V _c (cm/sec)	V _c /V _m
22.9	23.0	-1.87 × 10 ⁻³	-2.91 × 10 ⁻³	1.56
	27.9	-1.84 × 10 ⁻³	-3.50 × 10 ⁻³	1.90
	35.4	-2.27 × 10 ⁻³	-4.50 × 10 ⁻³	1.98
23.0	13.7	-1.41 × 10 ⁻³	-1.76 × 10 ⁻³	1.24
	23.0	-1.76 × 10 ⁻³	-2.97 × 10 ⁻³	1.69
	39.6	-2.87 × 10 ⁻³	-4.92 × 10 ⁻³	1.72
27.9	20.9	-1.43 × 10 ⁻³	-2.63 × 10 ⁻³	2.02
	28.0	-3.36 × 10 ⁻³	-2.67 × 10 ⁻³	1.09
	61.7	-6.70 × 10 ⁻³	-8.08 × 10 ⁻³	1.20
28.3	19.9	-1.80 × 10 ⁻³	-2.69 × 10 ⁻³	1.50
	33.1	-3.65 × 10 ⁻³	-4.46 × 10 ⁻³	1.22

$$V_c = \frac{2}{3\mu(3\mu' + 2\mu)} \left[\left(-\frac{d\gamma}{dT} \right) \frac{dT}{dx} R\mu + (\rho' - \rho) gR^2(\mu + \mu') \right]$$

TABLE 3. VALUES OF V_c/V_m OBTAINED WITH MAXIMUM MEASUREMENT ERRORS OF VELOCITY AND RADIUS

Velocity (cm/sec) Radius (μm)	-1.29 × 10 ⁻³	-1.43 × 10 ⁻³	-1.57 × 10 ⁻³
19.1	2.04	1.84	1.68
20.9	2.23	2.02	1.84
22.7	2.42	2.19	1.99

ORIGINAL PAGE IS
OF POOR QUALITY

REFERENCES

1. Ang, C. Y. and Lacy, L. L.: **Monotectic and Syntectic Alloys, Experiment MA-044. ASTP Preliminary Technical Report, NASA TMX-64956, September 1975.**
2. Ang, C. Y. and Lacy, L. L.: **AIAA Progress in Astronautics and Aeronautics. Vol. 52, 1977, p. 523.**
3. Gelles, S. H., Collings, E. W., Abbott, W. H., and Maringer, R. E.: **Analytical Study of Space Processing of Immiscible Materials for Superconductors and Electrical Contacts. NASA Contract Report, NASA CR-150156, January 1977.**
4. Lacy, L. L. and Otto, G. H.: **AIAA Journal, Vol. 13, 1975, p. 219.**
5. Lacy, L. L., Nishioka, G., and Ross, S.: **UAH/NASA Workshop on Fluids Experiment System. J. Hendricks and B. Askins (editors), The University of Alabama in Huntsville, 1979.**
6. Johnston, M. H., Griner, C. S., Parr, R. A., and Robertson, S. J.: **The Direct Observation of Unidirectional Solidification as a Function of Gravity Level. Journal of Crystal Growth, Vol. 50, 1980, pp. 831-838.**
7. Cahn, J. W.: **Trans. Metall. Soc., AIME Vol. 242, 1968, p. 166.**
8. Goldberg, W. I., Shaw, C., Huang, J. S., and Pilant, M. S.: **J. Chem. Phys. Vol. 68, 1978, p. 484.**
9. Ostwald, W.: **Z Phys. Chem., Vol. 34, 1900, p. 495.**
10. Lacy, L. L. and Ang, C. Y.: **Apollo-Soyuz Test Project Summary Science Report. Vol. I, NASA SP-412, 1977, p. 403.**
11. Gelles, S. H. and Markworth, A. J.: **Space Processing Applications Rocket Project, SPAR II Final Report. NASA TM78125, November 1977.**
12. Lacy, L. L. and Otto, G. H.: **The Stability of Liquid Dispersions in Low Gravity. AIAA/AGU Conference on Scientific Experiments on Skylab, Huntsville, Alabama, November 1974, AIAA Paper 74-1242.**
13. Nishioka, G. M., Lacy, L. L., and Facemire, B. R.: **The Gibbs Surface Excess in Binary Miscibility Gap Systems. J. Colloid and Interface Science, Vol. 80, No. 1, March 1981, pp. 197-207.**
14. Collier, R. J., Borekhardt, C. B., and Lin, L. H.: **Optical Holography. Academic Press, New York, 1971.**
15. Tyler, G. A. and Thompson, B. J.: **Optica Acta, Vol. 23, 1976, p. 685.**
16. van Ligten, R. F.: **Optics and Laser Technology, Vol. 1, 1969, p. 71.**
17. Thompson, B. J., Ward, J. H., and Zinky, W. R.: **Applied Optics, Vol. 6, 1967, p. 519.**

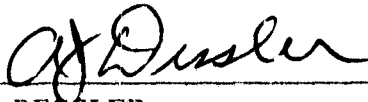
18. Silverman, B. A., Thompson, B. J., and Ward, J. H.: *J. of Applied Meteorology*, Vol. 3, 1964, p. 792.
19. Kurtz, R. L.: *The Techniques of Holographic Particle Sizing*. NASA Technical Report, NTR R-404, 1973.
20. Witherow, W. K.: *Holographic Microscopy Studies of Emulsions*. Master's Thesis, University of Alabama in Huntsville, 1981.
21. Witherow, W. K.: *Optical Engineering*, Vol. 18, 1979, p. 249.
22. Trolinger, J. D.: *Optical Engineering*, Vol. 14, 1975, p. 383.
23. Hawley, G. G. (editor): *The Condensed Chemical Dictionary*. Van Nostrand Reinhold Company, 1971.
24. Young, N. O., Goldstein, J. S., and Block, M. J.: *J. Fluid Mech.*, Vol. 6, 1959, p. 350.
25. Thompson, R. F., DeWitt, K. J., and Labus, T. L.: *Chem. Eng. Commun.*, Vol. 5, 1980, p. 299.

APPROVAL

OPTICAL STUDIES OF A MODEL BINARY MISCIBILITY GAP SYSTEM

By L. L. Lacy, W. K. Witherow, B. R. Facemire, and G. M. Nishioka

The information in this report has been reviewed for technical content. Review of any information concerning Department of Defense or nuclear energy activities or programs has been made by the MSFC Security Classification Officer. This report, in its entirety, has been determined to be unclassified.



A. J. DESSLER
Director, Space Science Laboratory